Memoirs of the Faculty of Engineering, Nagoya University
Vol. 32, No. 1. (1980)

RELIABILITY-BASED DESIGN OF GEOTECHNICAL ENGINEERING PROBLEMS

MINORU MATSUO, AKIRA ASAOKA and KUNIO KAWAMURA

Depertment of Geotechnical engineering

(Received June 3, 1980)

Abstract

This paper describes the "Dynamic Design Procedure" of earth construction works. In the general design problems, all information needed for design is collected in advance and the design is completed before the construction. However, since many kind of uncertainties such as the analytical errors in idealization of the complicated real behavior, the variation of soil properties and insufficient information due to limited numbers of samples are inevitable in the results of design, it is far better from both view points of costs and safety in construction that we proceed with construction changing the previous design by using new information which can be obtained during construction. This advantage is specifically large in the earthwork problems because the change of design is comparatively easy. In the present paper, the process in which the previous design is changed by new information and the optimal design can be always led is called the "Dynamic Design Procedure" and formulated based on the Bayesian reliability prediction.

The stability problems of embankment and excavation are mainly taken up as the concrete examples of earth construction works.

CONTENTS

1. Introduction

The size of the recent earth construction works has become large and in addition, the works to poor ground have steadily increased. In design and construction of large-sized earth works, the following two points are specifically important. One is the quantitative evaluation of various uncertainties which occur in design and construction. The other is the optimization of design and construction under consideration from the mechanical and economical aspects. In order to satisfy the two points, a design method based on the reliability theory is applied to the design of large-sized earth works.

In this study, the authors propose the new design method "Dynamic Design Procedure" based on the reliability theory. The term "Dynamic Design" is used here in the meaning that the design depends on the time. The contents of this procedure are divided into three main parts as follow. The first step is to carry out the prior design before construction in order to decide the optimal action by using the soil test results and the statistical decision theory. That is, the safety of each alternative is quantitatively compared by the reliability and the evaluation of each alternative is done by the Bayes' risk-estimation in which the reliability is combined with cost, so that it is easy to obtain the people's consensus on the final result of the prior design. However, it is impossible to make the risk of failure zero during construction even if the prior design is the optimal at that situation. Even under such a condition, the excuse that the failure has unfortunately occured in spite of making the prior design optimal can not be allowed in public engineering

practice. So that civil engineers have to prevent the fatal damage such as an all-out failure by taking the quick countermeasures including the change of design if the sign of failure can be found during construction. Therefore, the second step is to find the good technique in order to evaluate the degree of safety and to predict the forthcoming failure during construction. In this paper, the authors propose the prediction methods in which the observed results obtained during construction are used.

In the third step, the optimal action of earth works decided in advance, in the first step before construction for example, is changed into the better action by the observed results newly gained after the construction begins. In other words, the optimal decision in design and construction is always modified by using the new information from the view point that civil engineers always make the earth construction works optimal. This point is the remarkable feature of the present method, because the modification of design is comparatively easy in earth works. Thus, the "Dynamic Design Procedure" is considered to be more effective than the traditional design works which usually finish in advance of construction and then can be called "Static Design Procedure" (Matsuo and Kuroda, 1975; Matsuo and Kawamura, 1975).

There are three major parts in this paper. In chapter 2, the statistical characteristics of soil properties related to the design of embankment and excavation at soft ground are discussed based on many date from soil tests.

Chapter 3 is concerned with the "Dynamic Design Procedure" for embankment construction works. It is firstly discussed how to improve the uncertain condition in stability analysis of slope by using the observed results during construction and the "Dynamic Design Procedure" is reasonably formulated by the dynamic decision process based on the Bayesian reliability theory. In addition, a lot of numerical examles are carried out and the optimal solutions obtained are tabulated for convenience in practical use.

In chapter 4, the optimization of prior design of excavation problem is described. That is, the method to decide the optimal action in the prior design is discussed based on the statistical properties of soils and the analytical error of the conventional design equations. The obtained optimal solutions are compared with the actual results of the past construction fields. The observational method to predict the actual failure of excavation field is proposed, which is used to change the prior design. In addition, the "Dynamic Design Procedure" which is formulated for embankment problem in chapter 3 is modified to able to apply to excavation problem and the results obtained from the numerical studies are compared with the actual excavation works.

In the final chapter, the main remarks of this paper are summarized.

2. Statistical characteristics of soil properties

When we attempt to use the reliability approach to the soil engineering field, it is necessary to study risk problems from two points of view. One is the study of the variability of natural soil properties (Hooper and Butler, 1966; Lumb, P., 1966, 1970; Lumb and Holt, 1970; Matsuo and Kuroda, 1972; Matsuo and Asaoka 1974; Schultze, 1975). In these investigations, the characteristics of the variability

are statistically examined with many actual data, and the probability density functions (pdf) of random soil properties are also statistically estimated. These results make it possible to obtain the relation between the safety index and the probability of failure. Studies on the transition of variability of soil properties due to consolidation (Matsuo and Asaoka, 1975) can also be used for the same analysis.

The other point of view is the study of the methods for an optimal design. According to the development of these studies, a rational decision for the scale of soil exploration and the magnitude of the safety index has gradually come to be possible.

In this chapter, the variability of strength of cohesive soils are discussed in detail.

It is well known that the data from soil explorations and laboratory tests usually show a large variation. This variation depends on many factors. Generally speaking, two kinds of variation are contained in these data: one is due to the physical nature of soils and the other is attributed to technical problems. All natural soils show variations in properties from point to point in the ground because the soils themselves have an inherent variation and, besides, the underground water table frequently changes. On the other hand, variation due to many kinds of technical problems is mixed up in the data. They are as follows:

(1) errors due to an engineer's judgement in which he regards different types of soil layers as the same layer.
(2) variation due to the difference in the samplers, the testing apparatus and the levels of workmanship in sampling and tesing.

Many investigations have been continued in order to make these variations and errors clear and distinguishable. Even if any effort is made, however, such variation due to the inherent properties or the chance errors cannot be completely excluded. This suggests the necessity of a stochastic approach to the soil engineering problems.

It should be noted that the data shown in this chapter do not include the above mentioned errors (Matsuo, et al., 1975).

2. 1. Variation of Mechanical Properties Related to Strength

2. 1. 1. Strength of Cohesive Soil

In saturated cohesive soils, the undrained strength or the unconfined compression strength ($=2c_u$) are most important. Generally speaking, it is considered that there are three types in the variation characteristics of the undrained strength of saturated cohesive soils (Matsuo and Kuroda, 1971, 1974):

Type Ⅰ: both the mean and the deviation are independent of depth
Type Ⅱ: the mean has a linear relation with depth, but the deviation is independent of depth
Type Ⅲ: both the mean and the deviation have linear relations with depth

Representing the conceptual diagrams, these three types will be shown as Fig. 2.1.

(1) Case of Type Ⅰ

The probabilistic variation characteristics of this type can be represented as follows:

$$c_u(z) = \mu + \sigma u(z) \tag{2.1}$$

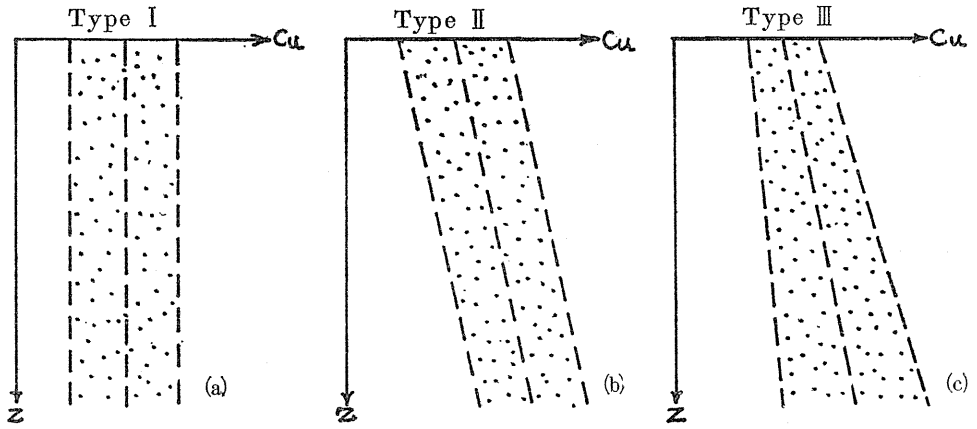

Fig. 2. 1. Typical Types of Distribution of c_u.

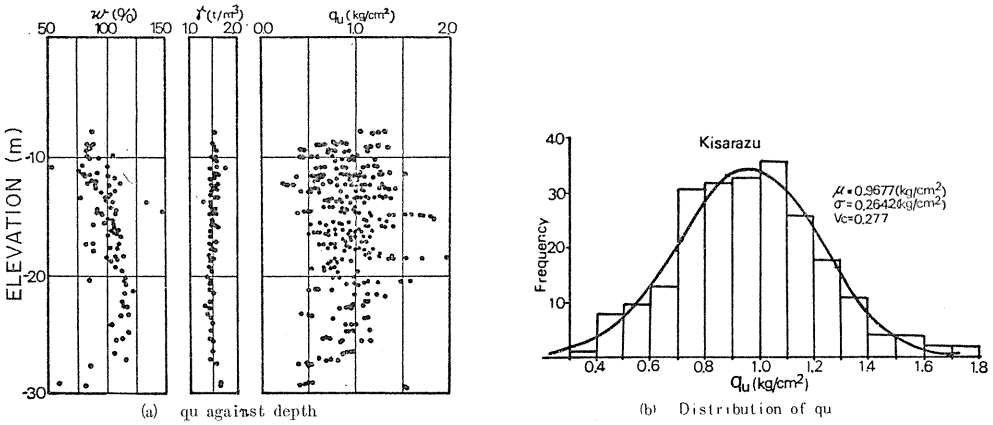

Fig. 2. 2. Variation of soil properties.

Table 2. 1. χ^2-test of q_u.

Sampling site	n	Vc	χ^2	f
Horikawabashi	119	0.181	16.1034	7
Kisarazu	231	0.273	8.0743	12
Neyagawa (1)	86	0.237	8.5055	7
Neyagawa (2)	98	0.259	12.4698	7
Yasuura	538	0.409	17.6745	12
Keihin	271	0.320	9.0946	10
Chiba	192	0.222	6.3492	4
Kinuura	127	0.373	8.8760	4

Note: n is the sample size of q_u.
f is the degree of freedom.

where z denotes the depth, μ the mean, σ the standard deviation and $u(z)$ the standardized normal random variable.

An example of variation of q_u against depth is plotted in Fig. 2.2 (a) and the frequency distribution is shown in Fig. 2.2. (b) which shows good agreement with the theoretical normal distribution. Much other data of clay layers of this type were similarly investigated. Some results are given in Fig. 2.3 and Table 2.1. Fig. 2.3 is a diagram on normal distribution paper and Table 2.1 gives the results of the χ^2-test. These figures and table show that the unconfined compression strength can be regarded as a normal random variable.

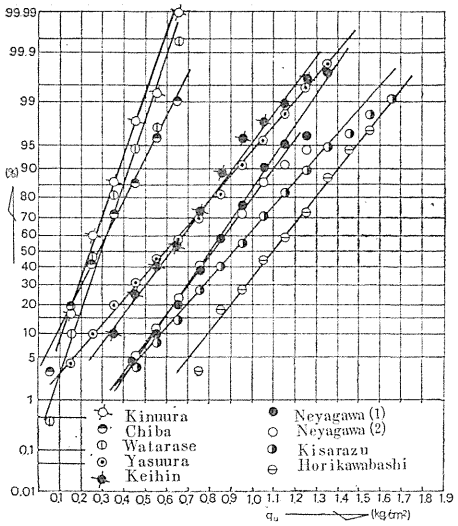

Fig. 2. 3. Distribution of q_u.

In Table 2.1, we should pay attention to the values of the coefficient of variation V_c. That is, they are restricted in a narrow range from 0.2 to 0.4 irrespective of the large difference in their mean values and standard deviations which can be read from Fig. 2.3. These results are supported by the results for different clays by Hooper and Butler (1966), Lumb (1966), Wu and Kraft (1967), Meyerhof (1970) and other researchers.

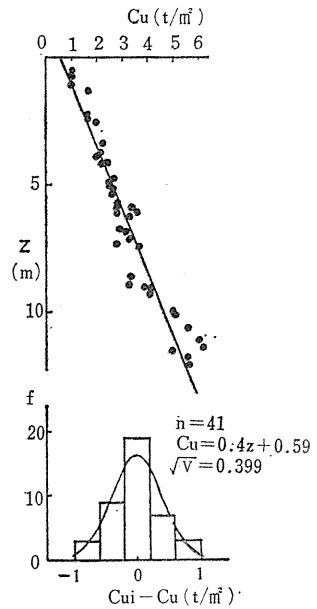

Fig. 2. 4. Distribution of c_u. (after Kurihara)

(2) Case of Type Ⅱ

The probabilistic variation of characteristics of this type can be written as follows:

$$c_u(z) = a + bz + \sigma u(z) \qquad (2.2)$$

where a and b are constant values. This type is frequently observed for normally consolidated clayey soils and statistically investigated in detail by Kurihara, for instance, by using the data of the Japanese Highway Public Corporation. Fig. 2.4 and Table 2.2 are the results reported by Kurihara (1972). Fig. 2.4 shows that the mean has a linear relation with depth, but the standard deviation is independent of depth and the frequency distribution follows the normal distribution. In Table 2.2, the values of the coefficient of variation are given with other data. It should be noted that these values for various clayey soils are limited within the narrow range from 0.2 to 0.4.

Table 2. 2. Statistical Properties of c_u.

Place	a (t/m²)	b (t/m³)	n	$\bar{c}_u$ (t/m²)	σ (t/m²)	Vc
Atsuki (1)	0.97	0.339	36	1.87	0.418	0.22
Atsuki (2)	0.59	0.401	41	1.52	0.339	0.26
Atsuki (3)	1.21	0.230	19	1.82	0.688	0.38
Atsuki (4)	1.25	0.245	60	2.06	0.567	0.28
Funako	1.24	0.153	52	1.59	0.486	0.30
Aiko	1.56	0.075	56	1.80	0.435	0.24
Takasaki (1)	1.10	0.194	60	1.61	0.584	0.35
Takasaki (2)	1.88	0.178	58	2.59	0.701	0.27
Kawaso	2·78	0.215	81	4.29	1.497	0.35
Fukuroi (1)	0·91	0.140	29	1.37	0.345	0.25
Fukuroi (2)	0·91	0.140	29	1.46	0.345	0.24
Toyota	2·78	0.579	40	3.93	1.216	0.28

Note: n is the sample size.
$\bar{c}_u$ is the average value of c_u. σ is the standard deviation.
Vc is the coefficient of variation. (after Kurihara)

(3) Case of Type Ⅲ

This type of variation in strength is also seen very frequently for normally consolidated clays. Fig. 2.5 is the results shown by Lumb (1966). He gave the following equation for this type:

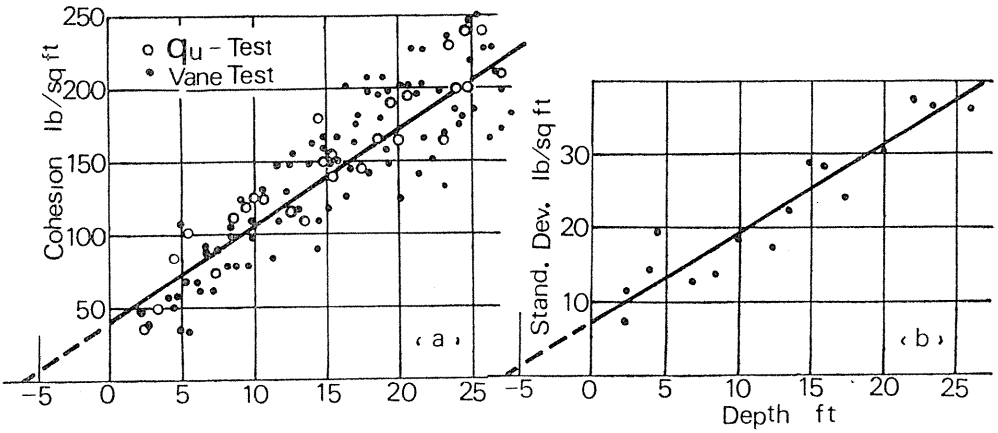

Fig. 2. 5. (c_u, σ_c~z) Relations. (after Lumb)

$$c_u(z)=\alpha' z+\beta'+(\alpha'' z+\beta'')\zeta(z) \tag{2.3}$$

where α' and β' are functions of the mean of the plasticity index, α'' and β'' are functions of the standard deviation of the plasticity index and $\zeta(z)$ is the standardized normal random variable. Fig. 2.6 shows the standardized variable $u=(c_u-$

$c_{uo})/\sigma_c$ which is plotted against the standardized normal variable $\zeta(z)$. This figure indicates that there is agreement with the normal distribution.

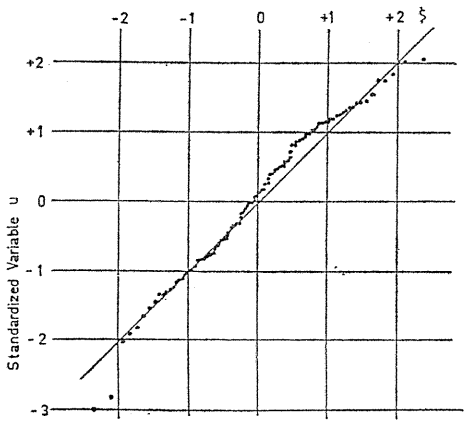

Fig. 2. 6. Distribution of u. (after Lumb)

2. 1. 2. Autocorrelation of Undrained Strength

As discussed thus far, soil properties vary from point to point and it is therefore necessary to investigate their correlation in the different positions. This nature of variation can be characterized by an autocorrelation.

The autocorrelation concerning the undrained strength of saturated clay is most important in a general stability analysis of embankment and excavation. In the previous section, we discussed three types of the variation of undrained strength of which each has an autocorrelation.

The autocorrelation $r(\tau)$ of $c_u(\boldsymbol{x})$ can be calculated as follows:

The general stochastic model of $c_u(\boldsymbol{x})$ is expressed by the following equation:

$$c_u(\boldsymbol{x})=\mu(\boldsymbol{x})+\sigma(\boldsymbol{x})\cdot u(\boldsymbol{x}) \tag{2.4}$$

where $c_u(\boldsymbol{x})$ is the measured undrained strength and $\boldsymbol{x}$ is the position vector. In practice, only one value of $c_u(\boldsymbol{x})$ can be measured at each position of the clay layer, and we assume this value as an outcome of a random variable which satisfies the following ergodic hypothesis:

$$\left.\begin{aligned} &E[c_u(\boldsymbol{x})]=\frac{1}{V}\int_V c_u(\boldsymbol{x})\,dV=\mu \\ &E[\{c_u(\boldsymbol{x})-\mu\}^2]=\frac{1}{V}\int_V \{c_u(\boldsymbol{x})-\mu\}^2 dV=\sigma^2 \\ &E[\{c_u(\boldsymbol{x})-\mu\}\{c_u(\boldsymbol{x}+\boldsymbol{\tau})-\mu\}] \\ &\quad=\frac{1}{V}\int_V \{c_u(\boldsymbol{x})-\mu\}\{c_u(\boldsymbol{x}+\boldsymbol{\tau})-\mu\}\,dV=r_c(\boldsymbol{\tau}) \end{aligned}\right\} \tag{2.5}$$

where V denotes the volume of the macroscopically homogeneous clay layer, μ and σ the spatial mean and the standard deviation of $c_u(\boldsymbol{x})$ in V, respectively, $r_c(\boldsymbol{\tau})$ the spatial autocorrelation coefficient of $c_u(\boldsymbol{x})$ and $\boldsymbol{\tau}$ the distance between the positions x_1 and x_2.

If normalized, the autocorrelation coefficient of $c_u(\boldsymbol{x})$ is defined as follows:

$$r(\tau)=\frac{r_c(\tau)}{\sigma(x)^2} \tag{2.6}$$

Fig. 2.7 shows $r(\tau)$ in the vertical direction, that is, in the case of $x=z$. Fig. 2.7 (a) corresponds to Type I in which case both μ and σ are independently

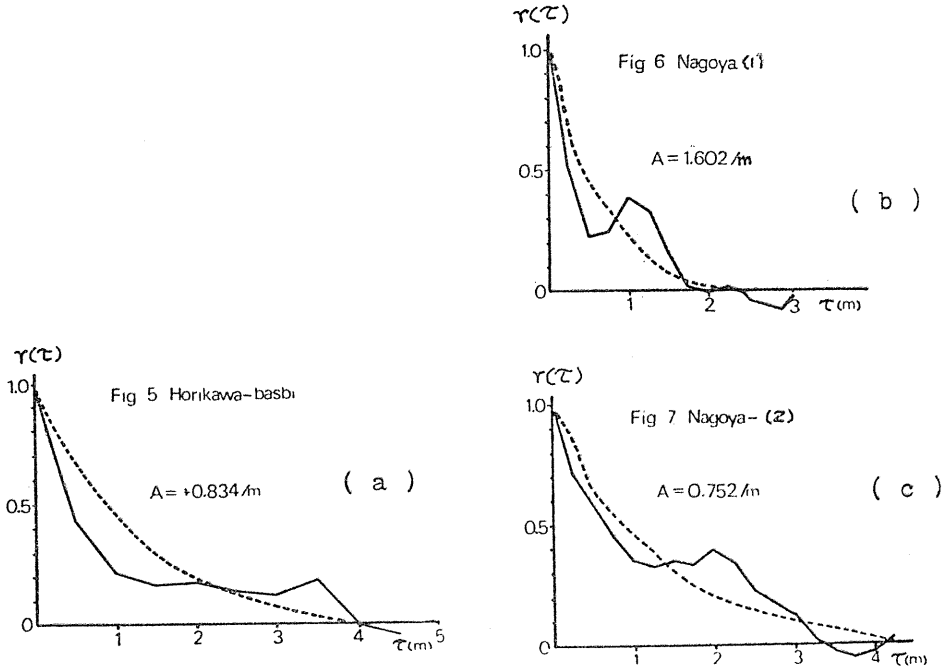

Fig. 2. 7. Autocorrelation in the vertical Direction.

constant against the depth. Fig. 2.7 (b) and (c) are those corresponding to Type II in which case $\mu(z)$ is linearly dependent upon the depth, but σ is independent of it. From these figures, it is expected that $r(\tau)$ can be expressed in the following form:

$$r(\tau)=\exp(-|A\tau|) \tag{2.7}$$

The dotted lines in Fig. 2.7 show the least squares fitting from Eq. (2.7). According to our data, including Fig. 2.7 in Matsuo and Asaoka (1976), Lumb and Holt (1970) and Wu (1974), the components of A are in the following range:

$$\left.\begin{aligned} A_z&=0.3-2.6\,(m^{-1})\\ A_h&\leq 0.01\,(m^{-1}) \end{aligned}\right\} \tag{2.8}$$

where A_z and A_h denote the coefficients in the vertical and the horizontal direction, respctively. It should be noted that the correlation of $c_u(x)$ in the horizontal direction is much stronger than that in the vertical direction. This means that the clays keep a very high homogeneity in the horizontal direction. On the other

hand, in the vertical direction, $r(\tau)$ generally becomes nearly equal to zero at the distance of $\tau=3-5$(m).

All these examples mentioned above are stationary cases in space. But the case of Type Ⅲ, given by Eq. (2.3), is very difficult because the random variable $\sigma(x)u(x)$ is not stationary in space. In this case, an accumulation of data is almost impossible for an actual problem and thus the calculated results have not been found yet. However, it is considered that $r(\tau)$ of Type Ⅲ is not very different from those of Type Ⅰ and Type Ⅱ.

2. 1. 3. Transition Process of Undrained Strength

The state of the strength condition may be changed from its initial state to another state due to consolidation. This causes a transition in the failure probability of an embankment. Therefore, it is very important to investigate the transition process, especially for multistaged construction of an embankment in which an increase in strength is expected in each stage of construction (Matsuo and Asaoka, 1975).

It has been observed by many researchers that the coefficient of variation of undrained strength is roughly constant in many natural clay layers (Lumb, 1966; Matsuo and Kuroda, 1974). The authors can also obtain the following relation from the theoretical formulation of transition process;

$$\frac{c_{u\,\mathrm{Ⅱ}}(x)}{c_{u\,\mathrm{Ⅰ}}(x)}=t(z) \tag{2.9}$$

where the random variable $c_{u\,\mathrm{Ⅰ}}(x)$ is the undrained strength before loading at the position vector x which represents a certain point in ground and $c_{u\,\mathrm{Ⅱ}}(x)$ that after consolidation by loading at the same point. Eq. (2.9) shows that the ratio of undrained strength after consolidation to the initial strength holds $t(z)$ constant. If the spatial mean and variance of strength are denoted as μ and σ^2 respectively, the following relations are demonstrated:

$$\left.\begin{aligned}\mu_{\mathrm{Ⅱ}}&=t(z)\,\mu_{\mathrm{Ⅰ}}\\ \sigma^2_{\mathrm{Ⅱ}}&=t(z)^2\sigma^2_{\mathrm{Ⅰ}}\end{aligned}\right\} \tag{2.10}$$

Eqs. (2.9) and (2.10) show that both the coefficient of variation of the strength at each depth and the spatial autocorrelation coefficient do not change before and after consolidation. This is very important in in engineering analysis.

Figs. 2.8 (a)-(e) show the distributions of c_u at Nagoya Port in Japan, where the embankment was constructed by the multistaged-loading method. Fig. 2.8 (a) shows the initial state of the clay layer before construction of the embankment and Fig. 2.8 (b) corresponds to the state just after the sand piles were driven into the clay layer in order to improve it. Figs. 2.8 (c)-(e) are the results after consolidation of each loading shown in the figures.

From these data, the constant $t(z)$ can be calculated by using Eq. (2.10). The computed results are shown in Fig. 2.9. In the figure, the full and dotted lines represent the mean ratio and the deviation ratio, respectively. All of the data of c_u within the range of each 5 m thickness of the clay layer are used in order to calculate μ and σ at depth z in each loading stage because of the lack of data at the same depth.

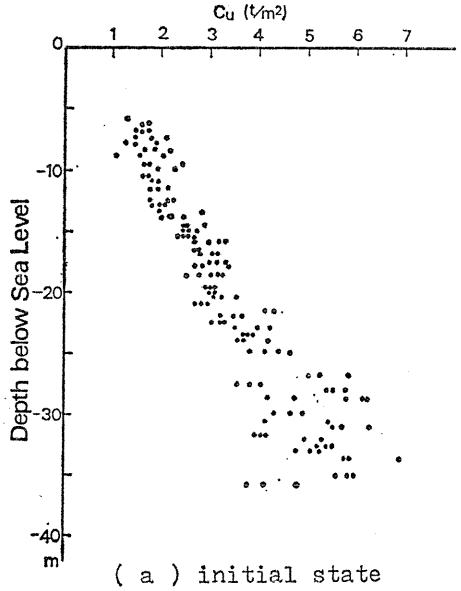

(a) initial state

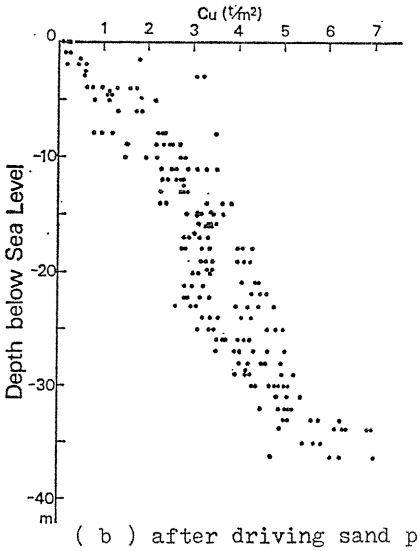

(b) after driving sand piles

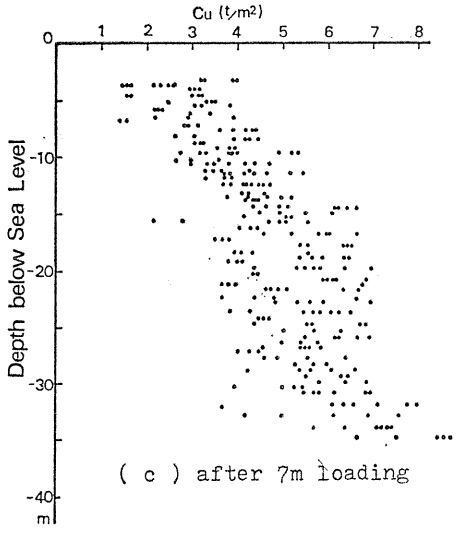

(c) after 7m loading

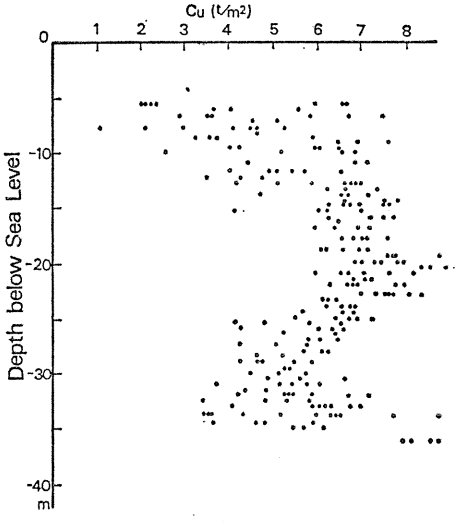

(d) after 12m loading

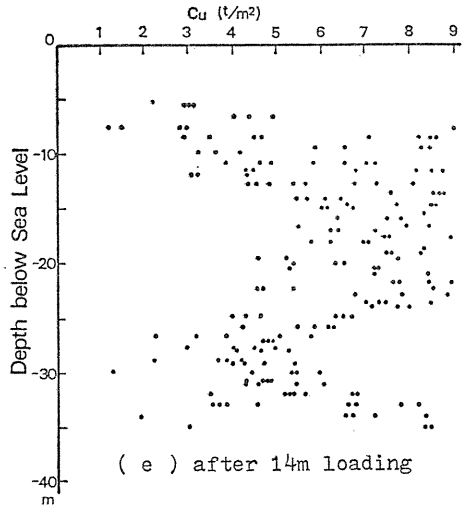

Fig. 2. 8. Relation between c_u and z.

According to this figure, the mean ratio and the deviation ratio provide suitable agreement with each other. That is, these results support Eqs. (2. 9) and (2 10).

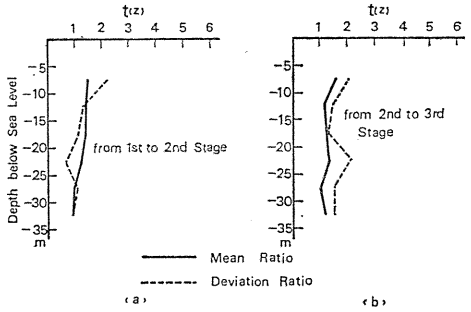

Fig. 2. 9. Ratio of Mean and Standard Deviation to Those of the Directly Former State.

2. 2. Variation of Unit Weight

Figs. 2. 10 (a) and (b) give an example of the distribution of the unit weight γ_t of a saturated natural clay layer at Kisarazu Port. Fig. 2. 10 (a) is this distribution in relation to the depth and Fig. 2. 10 (b) is its frequency diagram. Table 2. 3 shows the results of χ^2-tests for other saturated clay layers. From these figures and table, we can regard the distributions of γ_t as normal distributions.

From Fig. 2. 10 and Table 2. 3, it is concluded that the coefficient of variation of the unit weight is almost restricted in the range from 0. 02 to 0. 08. As was already seen in the previous section, this value is much smaller than that of the undrained shear strength of clay, that is, approximately one-tenth of it. This is very important in the analysis of failure probability of an embankment, as will be shown later.

Finally, studies on variation of mechanical properties for other soil parameters

are listed in the reference at the end of this paper which might give much convenient in engineering practice if necessary.

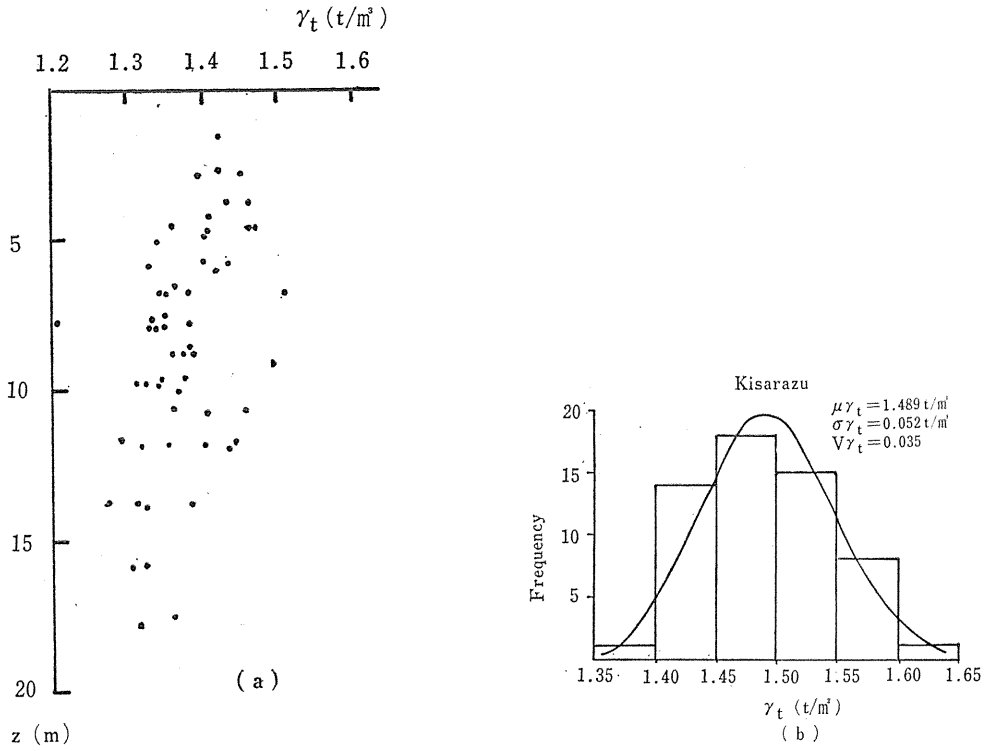

Fig. 2. 10. Distribution of γ_t.

Table 2. 3. χ^2-test of γ_t

Sampling site	n	V	χ^2	f
Horikawabashi	35	0.025	1.2080	2
Kisarazu	57	0.035	3.6837	4
Neyagawa (1)	34	0.023	0.0344	2
Neyagawa (2)	43	0.026	0.6915	3
Keihin	36	0.020	0.2915	2
Ichiba	25	0.031	1.8723	3
Shiogama	27	0.037	7.7148	5

Note: n is the sample size of γ_t. f is the degree of freedom.

3. Dynamic Design Procedure of Embankment

The present chapter discusses the dynamic methodology of reliability-based design on embankment problems including the transition process of undrained strength due to consolidation in a ground (Matsuo and Asaoka, 1978). The term "Design" is used here in a broad sense involving the observation and the modification of design during construction. To carry out this design philosophy, some preliminary remarks will be given in the first section.

3. 1. Preliminary Remarks

3. 1. 1. Reliability Analysis of Slope Stability

The probabilistic description of slope stability is given by positing the safety factor as a random variable. The safety factor of slope stability may include two kinds of random variables (Matsuo and Asaoka, 1976). One is error caused by many mechanical assumptions which are inevitable in a conventional $\phi_u=0$ and circular slip surface analysis, and the other comes from the probability model of c_u (undrained strength) which represents the heterogeneity of natural ground. From this point of view, the true safety factor F is given by

$$F=G+e \tag{3.1}$$

$$G=\frac{\mu}{a}+\varepsilon \tag{3.2}$$

where G denotes a safety factor based on $\phi_u=0$ analysis, e an analytical error of G, a an average shear stress on a slip circle (sometimes referred to as the design strength of the ground), μ the spatial mean of c_u and ε the random variable with zero mean. Using the spatial variance, σ^2, and a spatial covariance, $\sigma^2 r(\tau)$ of the undrained strength c_u, the variance of ε is demonstrated as follows;

$$\sigma_\varepsilon{}^2=\sigma^2\iint r(\tau)\,dLdL'/a^2L^2\equiv\sigma^2/\delta$$

where $r(\tau)$ denotes a spatial auto-correlation function of c_u, τ correlation length and L the length of a slip circle.

After the authors' study and the examinations of previous chapter on the probability model of c_u (Matsuo and Asaoka, 1977), ε can be regarded as a normal random variable and the parameters of which are made up to (μ, σ^2, δ) and a. The set of parameters, (μ, σ^2), is called the state of ground and is sometimes written as θ for simplicity:

$$\theta=(\mu,\ \sigma^2) \tag{3.3}$$

The value of δ can be explained to represent the number of strata through which the slip circle passes and the strengths are statistically independent of each other (Matsuo and Asaoka, 1976). The average shear stress on a potential slip circle, a, is related only to the weight of an embankment which we can determine and then a can be called as an engineer's action. When the value of μ is equal to a, the

expected value of G, $E[G]$, becomes 1, and therefore a is sometimes also referred to as the design strength of the ground.

Next discussion is concerned with an analytical error, e. Even though the ground is perfectly homogeneous and σ_ε^2 is equal to zero, there might be some inherent error caused by the mechanical assumptions adopted in the $\phi_u=0$ and circular slip surface stability analysis. By re-examining the case-histories of slope failure, a histogram of an approximate value of e can be obtained. That is, the value of each e is calculated backward by the following equation·

$$e=1-\hat{G} \tag{3.4}$$

where $\hat{G}$ is a estimated value of G by the conventional $\phi_u=0$ method. The results are summarized in the histogram in Fig. 3.1 (Matsuo, 1976), the shaded part of which indicates the data from 17 case histories of failures of embankments on soft clay layers in Japan. The other part of the figure is the computed results obtained from rearrangement of the data presented by Bishop and Bjerrum (1960) who analyzed 22 end-of-construction failures of footings and fills on saturated clay foundations. This figure suggests that the analytical error associated with the $\phi_u=0$ method is fairly small and is distributed evenly in the ranged of $-0.1\sim0.1$. In this paper, the parameter of the analytical error e is written by the following symbols:

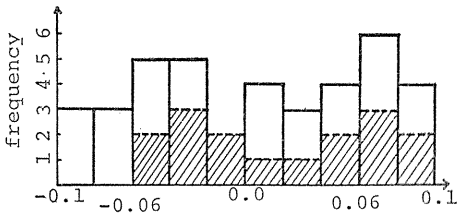

Fig. 3. 1. Histogram of analytical error, e.

$$\theta_e=(\mu_e,\sigma_e^2) \tag{3.5}$$

where μ_e and σ_e^2 are the mean and the variance of e respectively.

The state of nature which is considered in this paper is the set of unknown parameters (θ, θ_e), and this is written as $\underline{\theta}$ for convenience sake, that is,

$$\underline{\theta}=(\theta, \theta_e) \ : \text{a state of nature} \tag{3.6}$$

The probability of failure of an embankment is defined as the function of both a state of nature, $\underline{\theta}$, and our action, a:

$$\left.\begin{aligned} P_F(\underline{\theta}, a) &= \text{Prob.}\ (F\leq 1|\underline{\theta}, a) \\ &= \int_{F\leq 1} p(F|\underline{\theta}, a)\,dF \end{aligned}\right\} \tag{3.7}$$

which means the probability of $F\leq 1$ conditioned by $\underline{\theta}$ and a. In this paper, the statistical independence of ε from e is assumed.

3. 1. 2. Loss Functions and Predictive Failure Probability

A reliability-based design of soils can be regarded as a decision problem under conditions of uncertainty of a state of nature, $\underline{\theta}$, and then if the loss function is appropriately determined as a function of both $\underline{\theta}$ and an engineer's action, a, the design becomes suitable for application of the statistical decision theory. In that case, the optimal design is generally given by minimizing the expected value of a

loss function with respect to the state of nature, $\underline{\theta}$, (Bayesian decision criterion). A loss function is a criterion function of design and the simplest one is taken to be

$$L(\underline{\theta},\ a)=C_C(a)+C_F(a)P_F(\underline{\theta},\ a) \tag{3.8}$$

where $C_C(a)$ is the construction cost and $C_F(a)$ is the cost of failure.

To describe the uncertainty of a state of nature, $\underline{\theta}$, is generally regarded as a set of random variables in Bayesian statistics. Letting $\zeta(\underline{\theta})$ be the probability density function of $\underline{\theta}$, the expected value of $L(\underline{\theta},\ a)$ can be written as follows:

$$\left.\begin{aligned} r(\xi,\ a)&=\int\xi(\underline{\theta})L(\underline{\theta},\ a)d\underline{\theta}\\ &=C_C(a)+C_F(a)\int P_F(\underline{\theta},\ a)\xi(\underline{\theta})d\underline{\theta}\end{aligned}\right\} \tag{3.9}$$

The last term of Eq. (3.9) is the expected value of failure probability. Defining $P_F(a)$ as

$$\tilde{P}_F(a)=\int P_F(\underline{\theta},\ a)\xi(\underline{\theta})d\underline{\theta} \tag{3.10}$$

$\tilde{P}_F(a)$ can be referred to a Bayesian predictive-failure probability under conditions of uncertainty of $\underline{\theta}$. It is noteworthy that if we adopt the a^* as an optimal design with the knowledge of $\xi(\underline{\theta})$, this is equivalent to saying that we have already predicted the failure probability, $P_F(a^*)$, as an optimal one.

3. 1. 3. *Modification of $\xi(\underline{\theta})$ by Information obtained during Construction*

Since the apriori knowledge of a state of nature, $\underline{\theta}$, is still limited, the prior probability density function, $\xi(\underline{\theta})$, should be corrected and modified to the posterior probability density function by using information which can be obtained after construction begings. Observations during construction can be utilized as information about $\underline{\theta}$ only when the likelihood function of $\underline{\theta}$ can be defined by observation results.

Now it is necessary to consider a kind of information about $\underline{\theta}$ which is much applicable for engineering practice. The failure probability

$$P_F(\underline{\theta},\ a)=\int_{F\leq 1}p(F|\underline{\theta},\ a)dF$$

can also be regarded as a cumulative probability density function of mean shear stress a on a potential slip surface which is conditioned by $F=1$ and $\underline{\theta}$. Let us examine the meaning of this function next.

Since the failure probability is a monotone increasing function of a, the conjugate cumulative distribution fnction of a with respect to $F\leqq 1$ can be defined by the next equation:

$$CP(a|\underline{\theta})=\frac{\text{Prob.}(F\leq 1|\underline{\theta},a)}{\lim\limits_{a\to\infty}\text{Prob.}(F\leq 1|\underline{\theta},\ a)} \tag{3.11}$$

in which CP denotes the conjugate probability. But the denominator of this equation takes the value of 1, so the definition (3.11) becomes simply as follows:

$$CP(a|\underline{\theta}) = P_F(\underline{\theta},\ a) \tag{3.12}$$

It is obvious that

$$\lim_{a\to 0} CP(a|\underline{\theta}) = 0$$

so the domain of a is defined as $0<a<\infty$.

The definition from Eq. (3.11) or (3.12) expresses another aspect of a failure probability. Let us assume that a clay foundation is under the condition of Eq. (3.13) because of the load by an embankment corresponding to a mean shear stress a on a potential slip surface:

$$F = 1-\Delta,\ \Delta>0 \tag{3.13}$$

It can be demonstrated that for any given Δ, there exists the mean shear stress a' which is less than a and the positive Δa which uniquely satisfy

$$F=1 \text{ when } a'=a-\Delta a,\ \Delta a>0 \tag{3.14}$$

because

$$F=(\mu/a)+\varepsilon+e$$

is a monotone decreasing function of a, that is, there is a one-to-one relation between Δ and Δa. In actuality, the condition of a clay foundation can never exist, since the condition of Eq. (3.14) has already occurred before the state of Eq. (3.13) and at that time the clay foundation failed. In other words, the construction process of an embankment is the decreasing process of F from $+\infty$ to 1, which is equivalent to the increasing process of a and therefore the probability defined by Eq. (3.11) or (3.12) showes the cumulative probability density of a', which is less than a.

The differentiation of $CP(a|\underline{\theta})$ with respect to a yields the probability density function of a', which is denoted here by

$$\left.\begin{aligned} cp(a|\underline{\theta}) &= \frac{\partial}{\partial a} CP(a|\underline{\theta}) \\ &= \frac{\partial}{\partial a} P_F(\underline{\theta},\ a) \end{aligned}\right\} \tag{3.15}$$

Now, suppose that the embankment remains in a safe condition, $F>1$, until the design strength a reaches s, and when a becomes equal to s we can observe the signs of failure of the embankment. Since the likelihood function of $\underline{\theta}$ conditioned by the information s already can be defined by Eq. (3.15). In this case, the prior probability density function $\xi(\underline{\theta})$ can be corrected by using the Bayes theorem, as follows;

$$\xi(\underline{\theta}|F>1 \text{ when } a<s \text{ and } F=1 \text{ when } a=s) = \frac{cp(a=s|\underline{\theta})\xi(\underline{\theta})}{\int \text{numerator}\ d\underline{\theta}} \tag{3.16}$$

Similarly, when an error exists in observing information s, we can rewrite Eq. (3.16) as follows:

$$\tilde{\xi}(\underline{\theta}|F>1 \text{ when } a<s \text{ and } F=1 \text{ when } s<a<s+\Delta s)=\frac{\left[\int_{s}^{s+\Delta s} cp(a|\underline{\theta})da\right]\tilde{\xi}(\underline{\theta})}{\int \text{numerator } d\underline{\theta}}$$

$$=\frac{\{P_F(\underline{\theta},\ s+\Delta s)-P_F(\underline{\theta},\ s)\}\tilde{\xi}(\underline{\theta})}{\tilde{P}_F(s+\Delta s)-\tilde{P}_F(s)} \tag{3.17}$$

in which Δs denotes the observation error.

Information s is regarded the failure load conditioned by $F=1$. Therefore, the practical method to exactly predict the failure load is needed (Matsuo et al., 1977). In 3.3 of this chapter, the diagram for construction control of embankment on soft ground which makes it possible to successfully predict s by using the observational results is proposed as failure prediction technique.

3. 2. *Optimization of Dynamic Design*

Once information from observation is obtained during construction, the prior probabilty density function of the state of nature, $\underline{\theta}$, is naturally modified to the posterior one. Subsequent construction, therefore, should be based on the newly improved probability density function of $\underline{\theta}$. This means that the Bayes risk is re-evaluated by using the posterior probability density function, and if the optimal action which minimizes the posterior Bayes risk is largely different from the one before re-evaluation, the design is changed accordingly. In this paper, it will be shown that such a design process can be formulated by the statistical adaptive control theory in which a decision at any stage, including the initial one, is made by employing information which has already been gathered at that stage, and moreover, by naturally supposing the probability of receiving further information in future stages, on which future decisions will be based.

The design discussed here is an embankment construction on a saturated soft clay layer and therefore deciding the consolidation period is the main probrem, the intention being to increase the undrained strength of the clay layer. The construction is divided into several stages and a law embankment constructed in early stages is utilized as the consolidation load for later construction stages, and then will be left as it is for the period which has been chosen as necessary for the consolidation. A schematic diagram for this construction pro-

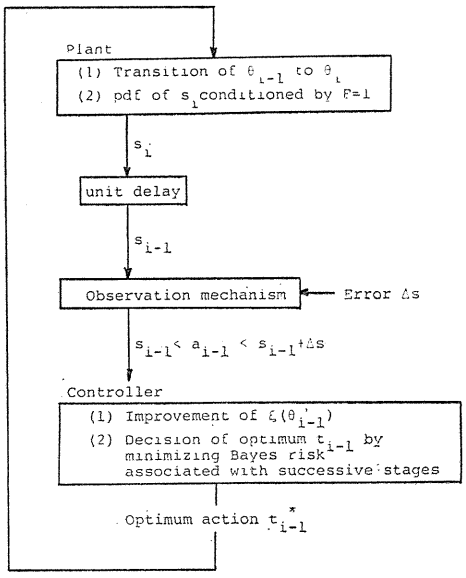

Fig. 3. 2. Optimization scheme of observational procedure.

cess is shown in Fig. 3. 2. When the observation information is obtained more than twice, the statistical independency of the observation is assumed. The information obtained in i-th stage is denoted by s_i and s^i, with super script i, represents the series of observations, $(s_1, s_2, \cdots s_i)$. The consolidation period after receipt of information from s_i is denoted by t_i which, in fact, is the action we should decide upon. In these cases, the loss function can be defined by $\underline{\theta}$ and $t^i=(t_1, \cdots t_i)$, because t^i determines the construction cost associated with the construction period. $t_1+\cdots\cdots+t_i$. The loss function defined in the final construction stage, the N-th stage, can be expressed as follows:

$$L(\underline{\theta}_N, t^N) \tag{3.18}$$

in which $\underline{\theta}_N$ can be derived from the following recursion equation which expresses the changing process due to consolidation, that is, from result in the previous chepter,

$$\underline{\theta}_{i+1}=T[\underline{\theta}_i, s_i, t_i] \tag{3.19}$$

(Matsuo and Asaoka, 1975 and 1977), and the result of which is

$$\underline{\theta}_N=\theta_N(\underline{\theta}, s^{N-1}, t^{N-1}) \tag{3.20}$$

in which $\underline{\theta}$ denotes the initial state of nature. Substituting Eq. (3.20) into (3.18), the loss function becomes

$$L(\underline{\theta}, s^{N-1}, t^N) \tag{3.21}$$

The Bayes rist computed at the final stage, ν_N can be expressed as follows:

$$\nu_N=\int\xi(\underline{\theta}|s^N)L(\underline{\theta}, s^{N-1}, t^N)d\underline{\theta} \tag{3.22}$$

in which $\xi(\underline{\theta}|s^N)$ can be obtained by using Eq. (3.16) or (3.17) recurrently, namely

$$\xi(\underline{\theta}|s^N)=\frac{cp(s_N|\underline{\theta})\xi(\underline{\theta}|s^{N-1})}{\int\text{numerator } d\underline{\theta}} \tag{3.23}$$

or

$$\xi(\underline{\theta}|s^N)=\frac{\{CP(s+\Delta s|\underline{\theta})-CP(s|\underline{\theta})\}\xi(\underline{\theta}|s^{N-1})}{\int\text{numerator } d\underline{\theta}} \tag{3.24}$$

Since both the series of observations s^N and the series of the past decisions t^{N-1} are available at the N-th stage, the optimal final decision t_N^* can be obtained as a function of s^N and t^{N-1}:

$$\nu_N^*=\min_{t_N|s^N,\ t^{N-1}}\nu_N=\int\xi(\underline{\theta}|s^N)L(\underline{\theta}, s^{N-1}, t^{N-1}, t_N^*)d\underline{\theta} \tag{3.25}$$

where

$$t_N^*=t_N^*(s_N,\ s^{N-1},\ t^{N-1}) \tag{3.26}$$

It is noteworthy that the denominator of Eqs. (3.23) and (3.24) represents the predictive probability density function of s_N and the predictive of $s_N<a<s_N+\Delta s$, respectively, both of which are conditioned by s^{N-1}. Let us express them by the following notations:

$$p(s_N|s^{N-1})$$

and

$$\text{Prob.}\ (s_N<a<s_N+\Delta s|s^{N-1})$$

Thus, the prediction of ν_N^* from the $(N-1)$-th stage yields the following.

$$\left.\begin{aligned}\nu_{N-1}&=E[\nu_N^*]\\&=\int p(s_N|s^{N-1})\nu_N ds_N\\&=\iint cp(s_N|\underline{\theta})\xi(\underline{\theta}|s^{N-1})L(\underline{\theta},\ s^{N-1},\ t^{N-1},\ t_N^*)d\underline{\theta}ds_N\end{aligned}\right\} \tag{3.27}$$

or

$$\nu_{N-1}=\sum_{s_{N-1}}\int\{CP(s_N+\Delta s|\underline{\theta})-CP(s_N|\underline{\theta})\}\xi(\underline{\theta}|s^{N-1})L(\underline{\theta},\ s^{N-1},\ t^{N-1},\ t_N^*)d\underline{\theta} \tag{3.28}$$

Since both s^{N-1} and t^{N-2} can be utilized at the $(N-1)$-th stage, by using Eq. (3.27) or (3.28), the optimal decision at $(N-1)$-th stage, t_{N-1}^*, can be obtained as the function of s^{N-1} and t^{N-2}, in the same way as t_N^*, that is,

$$t_{N-1}^*=t_{N-1}^*(s^{N-1},\ t^{N-2}) \tag{3.29}$$

Similarly, by working backward we have a series of optimal decisions which are functions of both past observations and past decisions:

$$t_i^*=t_i^*(s^i,\ t^{i-1}),\ i=1,\ \cdots,\ N \tag{3.30}$$

It is important to derive ν_0^*, the predictive Bayes risk calctlated in advance of construction which can be obtained by substituting Eqs. (3.30) of $i=1,\ \ldots,\ N$ into predictive form of ν_N:

$$\nu_0^*=E[\nu_N]=\int_{s_1}\int_{s_2}\cdots\int_{sN}\int_{\underline{\theta}}\prod_{i=1}^{N}cp(s_i|\underline{\theta})\xi(\underline{\theta})L(\underline{\theta},\ s^N,\ t^{N*})d(\underline{\theta},\ s_N,\ \cdots s_2,\ s_1) \tag{3.31}$$

or in the case of Eq. (3.17):

$$\nu_0^*=\sum_{s_1}\sum_{s_2}\cdots\sum_{sN}\int_{\underline{\theta}}\prod_{i=1}^{N}\{CP(s_i+\Delta s|\underline{\theta})-CP(s_i|\underline{\theta})\}\xi(\underline{\theta})L(\underline{\theta},\ s^N,\ t^{N*})d\underline{\theta} \tag{3.32}$$

So long as we employ the information s^i, actual failure is possible only after the final stage. When this is the case, the loss function has, instead of Eq. (3.8) the following form:

$$L(\underline{\theta}, s^N, t^{N*}) = C_C(\sum t_i^*) + C_F(\sum t_i^*) P_F(\underline{\theta}, a_f) \tag{3.33}$$

where a_f in the final term denotes the design strength related to the given dimension of an embantment being designed, and, therefore, is regarded as constant. C_C and C_F are related only to the total construction period. In this case, Eqs. (3.31) and (3.32) can be written simply as

$$\nu_0^* = C_C + C_F E[\tilde{P}_F] \tag{3.34}$$

in which $E[\tilde{P}_F]$ denotes the expected value of Bayesian predictive probability of failure with regard to probable future information.

Moreover, there generally exist restrictions on the construction period:

$$\sum_i t_i = T \ : \ \text{const.} \tag{3.35}$$

In this case, both C_C and C_F also become constant and the Eq. (3.34) can be obtained by

$$\left.\begin{aligned} \nu_0^* &= \min E[\nu_N] \\ &= C_C + C_F \cdot \min_{t_1 \cdots t_N} E[\tilde{P}_F] \end{aligned}\right\} \tag{3.36}$$

which allow us to conclude that a dynamic reliability-based design will intend to minimize the Bayesian predictive failure probability.

3. 3. Diagram for Construction Control of Embankment

An embankment on a soft ground is usually constructed by the smaller safety factor compared to other structures, because the change of design under construction is comparatively easy in the earth works. This makes it especially important in the embankment construction to control safely and quickly by using the information obtained from the practically possible measurements. As was discussed in the previous section, the information on the failure load (i. e. embankment height) conditioned by $F=1$ is especially important for the practical "Dynamic Design Procedure". This section describes the study on the method in which the degree of safety at the present situation is ascertained and the successive failure is predicted by observing the vertical settlement at the central place just under an embankment and the horizontal displacement near the toe of the slope.

3. 3. 1. Diagram for Prediction of Failure Proposed by the Authors

The deformation is an important index of the failure of a soft ground, as was mentioned before. The authors investigated from all aspects the process of displacements of saturated or almost saturated soft clay layers under many different embankments and found out that the plotting method of Fig. 3. 3 is especially useful in the effective and prompt prediction of the failure (Matsuo and Kawamura, 1977). In this figure, d is the vertical settlement at the central place just under an embankment and δ is the horizontal displacement near the toe of the slope. The process of displacement during construction of each embankment is plotted. The numerical values in this figure show the heights of the embankment. The followings are evident from this figure.

First of all, we should pay attention to the fact that the section and the unit

weight of each embankment, the soil properties and the thickness of each soft layer and other surroundings are different from each other, but many embankments under such different conditions failed near the one curve of this figure. Observing carefully the process of displacement in failure cases, this curve is approached as construction progresses, and on the other hand, in non-failure cases, there is a tendency to be distant from this curve, although it is approached once just after construction. To approach this curve means that the horizontal plastic flow is large compared to settlement by consolidation, and to deviate from this curve means that consolidation is predominant compared to the horizontal flow. That is, the embankment becomes safer. Accordingly, this curve can be regarded as the failure criterion line, and the failure of an embankment can be predicted by plotting the observed settlements and horizontal displacements on this diagram. Strictly speaking, the failure criterion curve does not come down to only one curve according to the theoretical and numerical consideration, but the difference is small as will be shown later and therefore, the one criterion line shown in Fig. 3. 3 is enough for practical use.

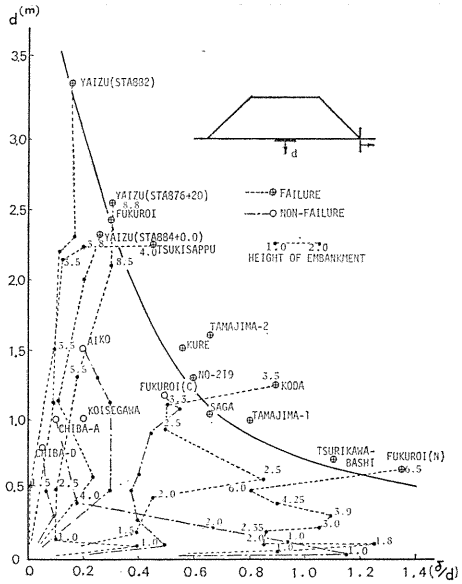

Fig. 3. 3. $(\delta/d \sim d)$ diagram for prediction of failure.

A few cases are examined in detail here. The *Koda* embankment, shown in Fig. 3. 3, is the failure example. This embankment was constructed on a typical alluvial clay layer 6 m in thickness whose undrained shear strength was about 2~3 (t/m^2). At first, banking was done continuously for about two weeks with 25 m in width and the height of embankment reached about 2.5 m. At that time, some cracks appeared on the surface of the embankment. This embankment was then left as it was for about three months in order to stop the progress of failure and to increase the shear strength of the clay layer. After that, the additional fill was banked. Suddenly, large cracks appeared on the slope and failure occured with the large horizontal displacement.

The displacement curve in Fig. 3. 3 shows this process. It was approaching to the failure criterion line for two weeks during the early stage of banking. This means that the horizontal plastic flow exceeded the settlement due to consoldation. During the second period, which lasted for three months, consolidation proceeded and the displacement curve tended to be a way from the failure criterion line; after construction of the additional fill, however, it went back toward the criterion line again and the failure finally occured near this line.

The *Chiba-A* embankment is a successful example of a embankment controled by the process presented in the diagram of Fig. 3. 3. The completed cross section of this embankment was 4 m high, 7.5 m wide at the top, 19.5 m wide at the base, and it was constructed on a soft clay layer which was 25 m in thickness. Banking was started at the speed of 0.25 m/day and was continued up to 1 m in height at

first. Since (δ/d) increased rapidly in these four days, as shown in Fig. 3. 3, banking was stopped for a while in order to examine the situation. The embankment was judged to be safe because d was very small although (δ/d) was large and, in addition to this, (δ/d) started to return to the left in Fig. 3. 3. Banking was continued at the original speed up to $4\,m$ in height because (δ/d) decreased continuously after that, while d gradually increased. After intended height was completed, the embankment was left as it was for more than one month. From Fig. 3. 3, it can be easily seen that the stabilization of this embankment increased during this period.

3. 3. 2. Examination by Total Settlements and Horizontal Displacements

Even if the engineering usefulness of the plotting method of Fig. 3. 3 is shown based on the actual measured data, the readers must have a question whether the macroscopic failure of a soft ground can be expressed by the settlement d at the only one point and the horizontal displacement δ at also the only one point of a ground. The following examination was done.

The macroscopic failure of a soft ground under an embankment is closely related to the total settlements and horizontal displacements as a whole ground which are shown by the area D and Δ in Fig. 3. 4. This fact can be intuitively accepted and was demonstrated also by the past actual data (Muromachi and Watanabe, 1962 for instance). That is, the measurd data showed that the degree of safety of a soft ground increased when consolidation of a whole ground was dominant, and at that time, D considerably increased while Δ hardly changed or slightly increased. On the other hand, when a ground approached to the failure, the increase of Δ was almost equivalent or more than that of D. The above mentioned fact suggests that D and Δ are better than d and δ as the fundamental index for the prediction of failure. Many measuring points, however, are necessary in order to obtain D and Δ. It always requires many workmen and the high cost, and often makes the pratical construction control of the long embankment on a soft ground impossible, for instance. On the other hand, measurement of d and δ is easy and therefore, the construction control by them is very advantageous in practice, if it is possible. Accordingly, the relationships between D and d and between Δ and δ are investigated on the basis of the actual data and the numerical examples in order to check whether d and δ can be used instead.

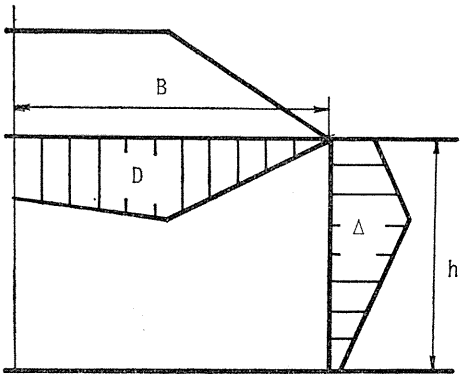

Fig. 3. 4. D and Δ in ground.

Fig. 3. 5 shows the relationships between them obtained by the measured values in the fields and Fig. 3. 6 the similar results by the numerical examples which will be explained later. It is evident from these figures that there are the strong linear correlations between D and d and between Δ and δ. Based on these results, in the following paragraph, the deformation characteristics on the $(d\sim\delta/d)$ diagram is investigated by the theoretical consideration and the numerical analysis.

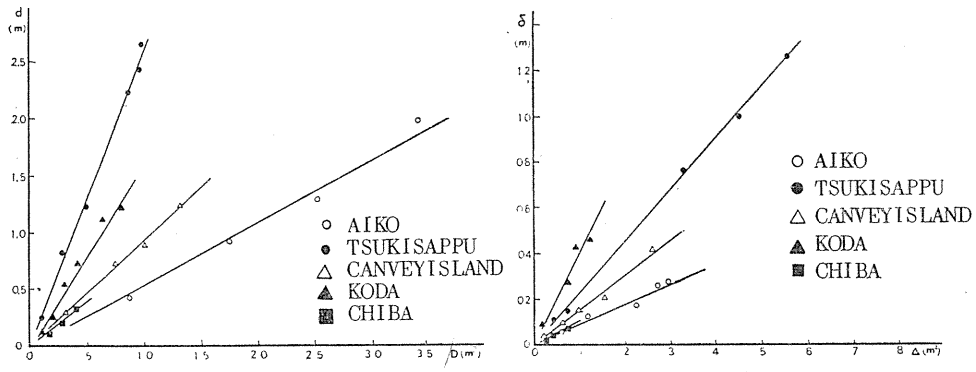

(a) $D \sim d$ (b) $\Delta \sim \delta$

Fig. 3. 5. Relation between D and d, Δ and δ in the measured values.

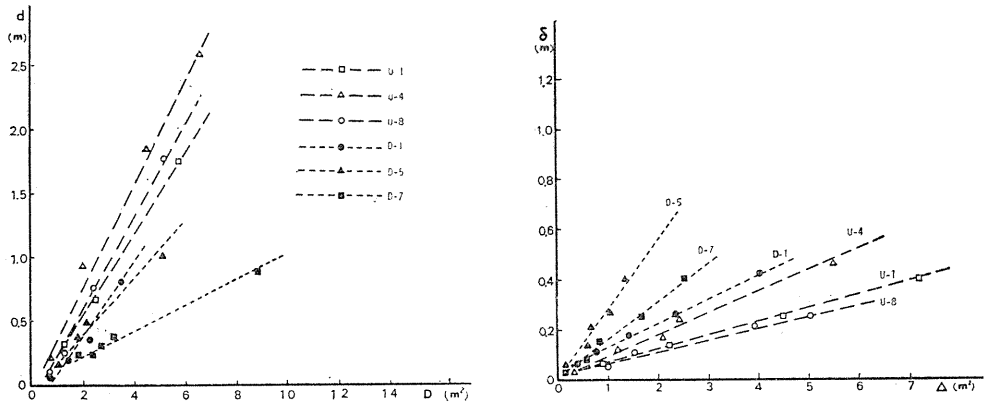

(a) $D \sim d$ (b) $\Delta \sim \delta$

Fig. 3. 6. Relation between D and d, Δ and δ in the numerical examples.

3. 3. 3. Idealization of Deformation Process

If an embankment is constructed on a soft clay layer, the deformation under the undrained condition generally occurs as well as deformation due to consoldation. This resultant behavior is so complicated that it is assumed here for the convenience of analysis that each deformation separately occurs.

In this paragraph, two typical, idealized cases are considered. One is the case in which only the deformation under the undrained condition generates. In this case, an embankment actually constructed as shown by a dotted line of Fig. 3. 7 (a) is idealized to be instantaneously banked up as a solid line. That is, it is assumed that the effective stress of an element in a layer rapidly changes from A to B in Fig. 3. 8 and only the undrained shear deformation correspondingly occurs. The other case is shown in Fig. 3. 7 (b). When the height of an embankment is large, it is rare to construct it rapidly in practice. The height of h_1, h_2, ..., h_n is usually banked up after each proper consolidation period. It is assumed here for this case that each height is instantaneously filled up and a clay layer is consolidated during the required term in each stage. That is, this case is idealized as the

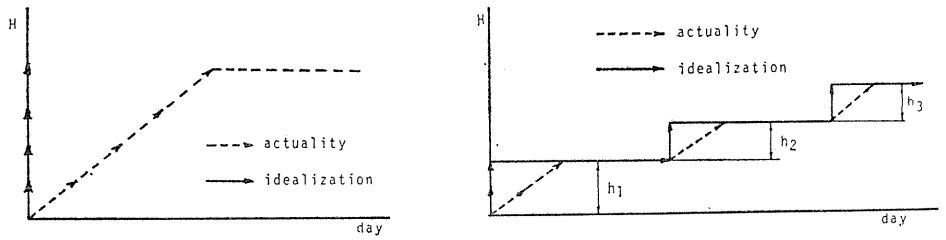

Fig. 3. 7. Idealization of behavior.

deformation under the undrained condition firstly occurs and after that, consolidation lasts, as shown by the process $A \rightarrow B \rightarrow C$ in Fig. 3. 8. The same idealization is used in study on the constitutive equation of soil and determination of the soil parameters in settlement analysis (Burland, 1971; Davis and Poulos, 1968).

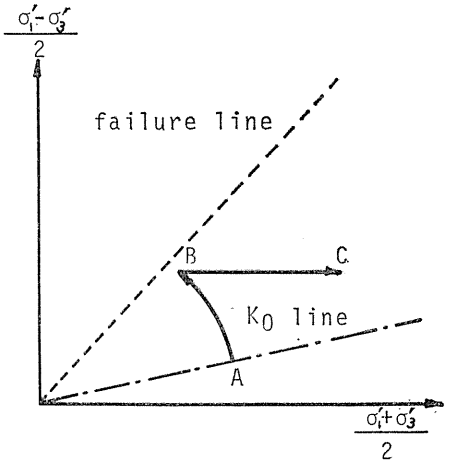

Fig. 3. 8. Idealized stress path.

The simplest method in the finite element so called, the Constant Strain Triangle Method, is applied to later analyses. Non-liner elastic analysis by Duncan and Chang (1970) is carried out with regard to the undrained shear deformation, and the elastic analysis is performed by using Biot's linear equation for the consolidation stage. The pore water pressure and displacement obtained under the undrained condition are used as the initial condition of consolidation stage. Strictly speaking, if the initial pore water pressure due to the constant increase of total stress under the undrained condition is applied, some errors occur, because the total stress changes during consolidation according to Biot's theory (Yamaguchi and Murakami, 1976). In addition to this, a question remains in the philosophy of calculation of total deformation because the linear elastic analysis is done against the consolidation process although the non-linear relationship is applied to the analysis of the undrained behavior. In the following, however, these errors are assumed small and neglected from the engineering view point.

(1) Comparison of Calculated Results under Undrained Condition with Observed Results

The Tsukisappu embankment already shown in Fig. 3. 3 is investigated here. This embankment was the test embankment which was constructed on a soft peat layer about 6 *m* in thickness. Since banking was rapidly done at an nearly constant speed without consolidation period, this embankment is taken up as a object of the

analysis under undrained condition. The observed result of the height of embankment, d, δ, Δu, D and Δ are shown by the solid lines in Figs. 3. 9 and 3. 10 respectively.

Let us compare these measured values with the calculated results by the finite element method. The soil parameters used in calculation were obtained by the undrained triaxial compression

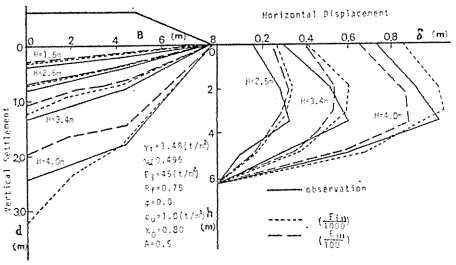

Fig. 3. 9. D and Δ at Tsukisappu.

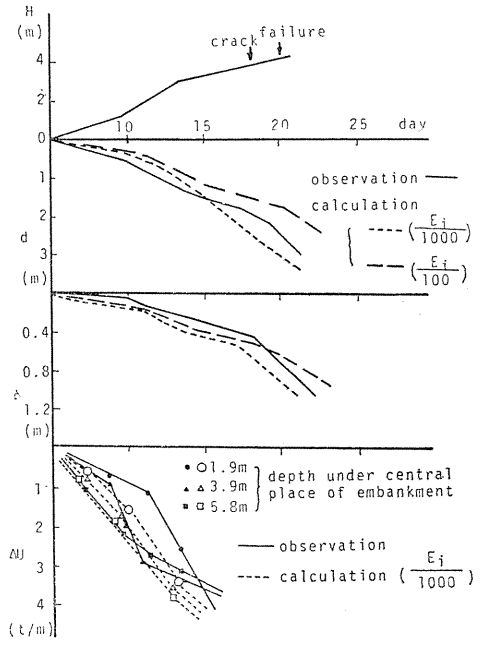

Fig. 3. 10. Progress of d, δ and Δu at Tsukisappu.

tests, which are shown in Fig. 3. 9. The values of pore pressure coefficient A and Poisson's ratio ν_u were assumed on the bases of past experience becauses the pore water pressure and Poisson's ratio were not measured. On the other hand, the test results of Young's modulus E_{tf} at failure were in the rang of (1/1000~1/100) E_i (E_i; the initial Young's modulus), but it was difficult to indicate the difinite value and therefore, the calculations were performed for both the cases of $E_i/1000$ and $E_i/100$, for reference. The calculated results are shown by the dotted and the broken lines in Figs. 3. 9 and 3. 10. The maximum difference of settlement d between the calculated and the observed results becomes nearly 35 cm at failure, but it is evident from these figures that they generally show very good agreement each other in magnitude and tendency. This suggests that the numerical investigation by the calculation method used here is reasonable. In the following paragraph, the calculations were performed for only condition of ($E_i/1000$).

(2) Comparison of Calculated Results under the Combined Condition of Undrained Behavior and Consolidation

The case of Fig. 3. 7 (b) whose stress path is given by the process $A \rightarrow B \rightarrow C$ of Fig. 3. 8 is discussed by Matsuo and Kawamura (1977) in detail. Let us compare the calculated results with observed results.

The Koda embankment shown in Fig. 3. 3 is examined in this section. The calculated and observed results during consolidation are shown in Figs. 3. 11. and 3. 12. The soil parameters and other conditions used in calculation are given in Fig. 3. 11. Fig. 3. 11 provides the comparison of the calculated results with the

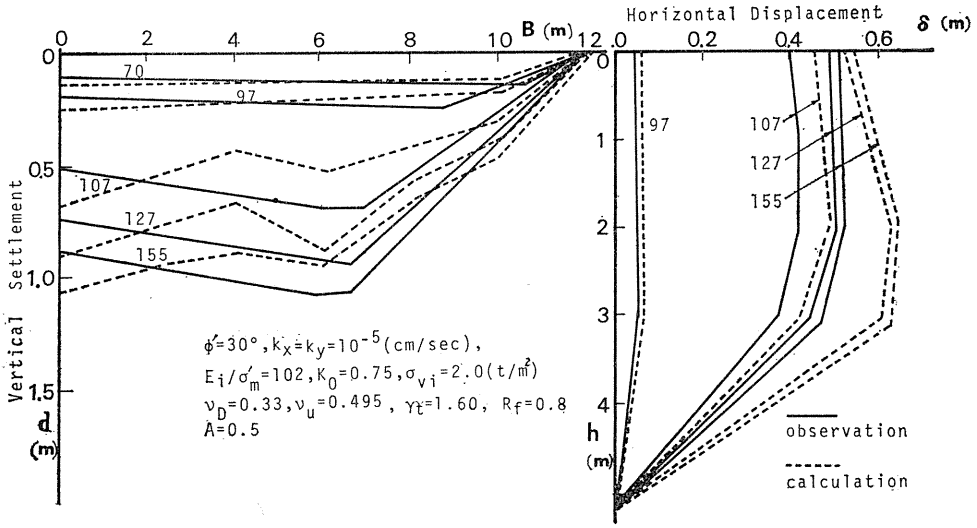

Fig. 3. 11. D and Δ at Koda.

observed results concerning D and Δ. The numerals in this figure show the number of days after construction started (refer to Fig. 3. 12). It is evident from Fig. 3. 11 that the calculated results agree quite well with the measured results. On the other hand, Fig. 3. 12 is the similar comparison with regard to d, δ and Δu. Speaking of the displacement, the calculated results generally become larger than the observed results, but the difference is only 25 cm in settlement and 7cm in horizontal displacement in maximum and thus, it can be judged that both results coincide well each other. The calculated pore water pressure is different by (1.5~2) t/m^2 from the measured one, but the tendency of calculated curve corresponds quite well to that of the observed one.

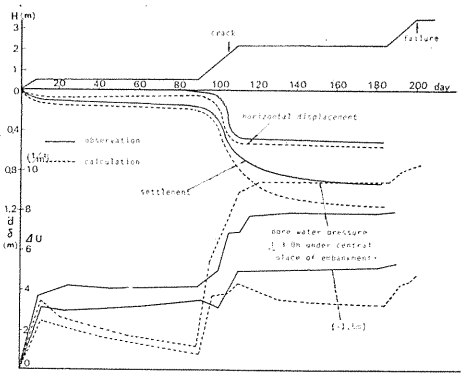

Fig. 3. 12. Progress of d, δ and Δu at Koda.

From these results, the numerical investigation by the present analytical method is considered very reasonable.

3. 3. 4. *Rearrangement of the* (d~δ/d) *Diagram*

The location and tendency of the final failure points which are the most important in the practical construction control are firstly investigated and next Fig. 3. 3 is modified to be able to use as the practical diagram for construction control.

(1) Location and Tendency of Final Failure Points

The final failure of a ground is defined at the rapidly increasing point of ($\Delta\delta/\Delta p$) on the (p~δ) curve which is nearly equal to the rapidly increasing point

of $(\Delta d/\Delta p)$ on the $(p\sim d)$ curve.

The failure points of all calculated cases and the observed cases of Fig. 3. 3 are summarized in Fig. 3. 13. The symbols in this figure, u and D mean the undrained condition and the combined condition, respectively and numeral shows the construction field number.

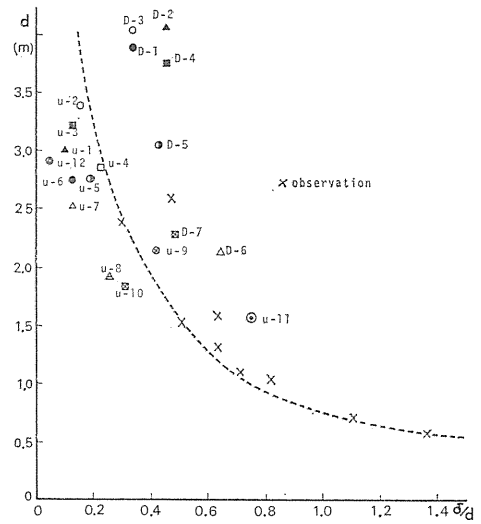

Fig. 3. 13. Location of failure points.

It can be seen from this figure that the failure criterion line obtained from the actual data can express also the calculated results on the whole. But the failure points under the combined condition of undrained behavior and consolidation are generally located beyond the curve and therefore, it might be possible to move the criterion line to a little upper position. From the engineering view point, however, it is better to consider the curve in Fig. 3. 13 as an upper limit of judgement of the failure. The reasons are as follows: (1) The calculated points under the undrained condition are located on or a little below this curve. (2) The ground is considered to practically behave in the state between the idealized undrained case and combined case of including consolidation. (3) The idealized undrained case adopted in analysis is perhaps on the safe side against the practical problem whereas the idealized consolidation case must be on the unsafe-side. This can be deduced also by the fact that the calculated settlement due to consolidation exceeds the observed one, as shown in Fig. 3. 12.

The following results relative to the location of the failure points should also be noted. In the cases of the large (B/h), they locate in the region of the large (δ/d) and the small d. On the other hand, the influence of the mechanical conditions such as K_0, σ_{vi}, c_u etc. on the deformation process and the location of a failure point on the $(d\sim\delta/d)$ diagram is not so large although they considerably affect on the relationship itself between a load and deformation (D'Appolonia et al., 1970; Höeg et al. 1968). This suggests that the $(d\sim\delta/d)$ diagram is very advantageous for practical use in the construction control.

(2) Modified Diagram for Construction Control

Fig. 3. 3 or Fig. 3. 13 is very useful by itself for the engineering problem, but it is insufficient yet to practically control the construction well by using it. That is, it is meaningless in engineering even if failure can be realized after it has occured. It is indeed necessary for the engineers to know the degree of safety of an embankment under construction and to quickly take the proper measures if signs of failure appear. Fig. 3. 3 or Fig. 3. 13 does not give the information on it. Fig. 3. 14 is one proposal of the construction controling diagram which is made under consideration on this point.

Each point and curve in this figure is obtained by the following method. The deformation process including each failure point was already found in the pre-

vious paragraph concerning the observed and the calculated examples. This means that the load p_j, the displacements d and δ in the j-th loading stage and the load at failure p_f of all displacement curves on the $(d\sim\delta/d)$ diagram are known. Therefore, it can easily indicate the points on each displacement curve which correspond to (p_j/p_f). These points are plotted in Fig. 3. 14 and each solid curve shows the approximate contour line of (p_j/p_f). The curve in Fig. 3. 3 or 3. 13 is adopted as the failure criterion line $(p_j/p_f=1.0)$.

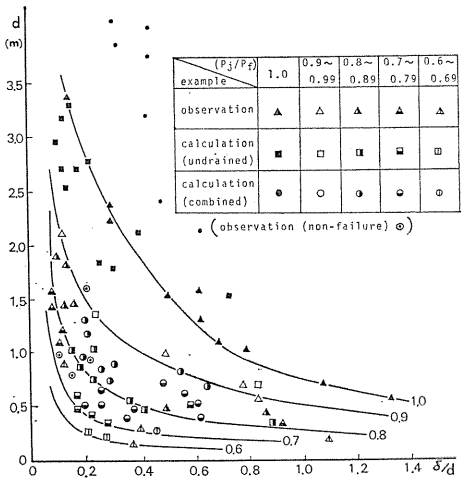

Fig. 3. 14. Modified $(\delta/d\sim d)$ diagram.

Firstly, it is noteworthy that the distance between each contour line becomes larger with increase of (p_j/p_f). This means that the deformation speed is accelerated as an embankment approaches to the failure. Accordingly, it is important for the engineers not to lose a chance to take measures quickly and smoothly such as a counterweight fill, removal of part of embankment, decrease in speed of construction and others. For this purpose, it is reasonable to consider the line of $(p_j/p_f)=0.9$ as a standard to judge, because it becomes evident from the minute examination of the construction records relative to the practical examples in Fig. 3. 3 that the points in which some cracks appeared on the top and the slope of embankment approximately correspond to $(p_j/p_f)=0.9$. These actual results are worthy to note.

It is needless to say that the movement of the displacement curve toward the smaller contour line shows the increase of stabilization of a ground due to consolidation.

The contour lines of (p_j/p_f) have been approximately obtained on the basis of the observed and the numerical examples, as was explained above. For the convenience of practical use, these curve are given in Table 3. 1 as the mathematical functions. We can safely control the construction of an embankment by plotting the displacements d and δ on Fig. 3. 14, since, at the present situation under construction, it is possible to predict the deformation process which is followed in the next step.

Table 3. 1. Mathematical function on contour line (P_j/P_f)

(P_j/P_f)	a	b	c	range of (δ/d)
1.0	5.98	1.28	−3.41	$0<\delta/d\leq 1.4$
0.9	2.80	0.40	−2.49	$0<\delta/d\leq 1.2$
0.8	2.94	4.52	−6.37	$0<\delta/d\leq 0.8$
0.7	2.66	9.63	−9.97	$0<\delta/d\leq 0.6$
0.6	0.98	5.93	−7.37	$0<\delta/d\leq 0.6$

$d=a\exp\{b(\delta/d)^2+c(\delta/d)\}$

3. 4. *Numerical Examples on Dynamic Design Procedure of Embankment*

The dynamic design shown thus far is actually carried out in the practical field based on the engineer's experience. In a sense, this empirical method has been formulated here and therefore the computed results often become very close to the performance of an engineer of ripe experience. However, the proposed method can give an objective risk assesment and then can obtain people's consensus widely. This is the especially advantageous point in this method. The numerical example shown here is prepared to help the understanding. The design condition employed is tabulated in Table 3. 2, which is so common in practice. That is, the embankment of $10m$ in height is constructed on the soft clay foundation whose compression test

Table 3. 2. Design Condition

Total banking height, H : 10m Construction period : 7 months Banking rate :30~35 cm a day Unit weight of banking material : 1.7 t/m^3 Stability number : 0.182
Compression test rerults of 30 samples Sample mean : 2.0 t/m^2 Sample standard deviation : 0.6 t/m^2 Auto correlation coefficient : $r(\Delta z)=\exp(-0.9\|z-z'\|)$ $\Delta z=\|z-z'\|$, z, z' : elevation (m)
Relation between degree of consolidation and time (use of sand drain piles) $U(t)=1-\exp(0.0275t)$, t : day $c_u/p=0.15$ coefficient of variation of c_u is constant during consolidation process (Matsuo and Asaoka, 1977)

results are also given in the table. The construction period is limited to 7 months at the longest. The banking rate is about $30\sim35\,cm$ a day and then 30 days are necessary for completion of $10\,m$ in height. Therefore only 6 months are available to increase the undrained strength of clay. In order to speed consolidation up, sand drains are used. The degree of consolidation as the function of time is also given in Table 3. 2.

The computed results of the optimal design which satisfy Eq. (3. 36) are tabulated in Table 3. 3 (a), (b) and (c). Through these table, the information s_i, the shear stress along slip circle, is converted into the banking height H_i at $F=1$. The observation errors Δs defined in Eq. (3. 17) is also changed to ΔH which is the error in measuring H_i. This means that we find the sign of failure when the banking height reaches to $(H_i\sim H_i+\Delta H)$. According to the observation of H_i, we can determine the appropriate period for consolidation t_i by using the design code of Table 3. 3. Table 3. 3(a) is the result of $\Delta H=50cm$. Table 3. 3(b) and (c) are corresponding to $\Delta H=25cm$ and $\Delta H=1cm$, respectively. The case of $\Delta H=10cm$ was also computed but the result agreed with the case of $\Delta H=25cm$. A typical construction process is shown in Fig. 3. 15 which is the illustration of the case with star marks in Table 3. 3(a). An engineer can decide his next action according

Table 3. 3. (*a*) Optimal design code when ΔH=50 cm

H_1 (m)	$t_1(H_1)$ (day)	H_2 (m)	$t_2(H_1, H_2)$ (day)	$t_3(H_1, H_2, H_2<H_3<10)$ (day)
5.0~5.5	18	5.5~6.5	81	81
		6.5~8.0	97	65
		8.0~8.5	113	49
		8.5~9.5	16	146
5.5~6.0*	18*	6.0~6.5	81	81
		6.5~8.0*	97*	65*
		8.0~9.0	113	49
		9.0~9.5	16	146
6.0~6.5	18	6.5~7.0	81	81
		7.0~8.0	97	65
		8.0~9.5	113	49
6.5~7.0	18	7.0~8.0	97	65
		8.0~9.5	113	49
7.0~7.5	18	7.5~8.0	97	65
		8.0~9.5	113	49
7.5~8.0	36	8.0~8.5	86	58
		8.5~9.5	101	43
8.0~10.0	36	$H_2>H_1$	101	43

Table 3. 3. (*b*) Optimal design code when ΔH=25 cm

H_1 (m)	$t_1(H_1)$ (day)	H_2 (m)	$t_2(H_1, H_2)$ (day)	$t_3(H_1, H_2, H_2<H_3<10)$ (day)
5.0~5.5	18	5.5~6.5	81	81
		6.5~8.0	97	65
		8.0~8.5	113	49
		8.5~9.5	16	146
5.5~6.0	18	6.0~6.5	81	81
		6.5~8.0	97	65
		8.0~9.0	113	49
		9.0~9.5	130	32
6.0~6.5	18	6.5~8.0	97	65
		8.0~9.0	113	49
		9.0~9.5	130	32
6.5~7.0	18	7.0~8.0	97	65
		8.0~9.0	113	49
		9.0~9.5	130	32
7.0~7.5	18	7.5~8.0	97	65
		8.0~9.0	113	49
		9.0~9.5	130	32
7.5~8.0	18	8.0~9.0	113	49
		9.0~9.5	130	32
8.8~10.0	36	$H_2>H_1$	101	43

Table 3. 3. (*c*) Optimal design code when $\Delta H=1$ cm

H_1 (m)	$t_1(H_1)$ (day)	H_2 (m)	$t_2(H_1, H_2)$ (day)	$t_3(H_1, H_2, H_2<H_3<10)$ (day)
5.0~5.5	18	5.5~6.5	81	81
		6.5~8.0	97	65
		8.0~9.0	113	49
		9.0~9.5	16	146
5.5~6.0	18	6.0~6.5	81	81
		6.5~8.0	97	65
		8.0~9.0	113	49
		9.0~9.5	130	32
6.0~6.5	18	6.5~8.0	97	65
		8.0~9.0	113	49
		9.0~9.5	130	32
6.5~7.0	18	7.0~8.0	97	65
		8.0~9.0	113	49
		9.0~9.5	130	32
7.0~7.5	18	7.5~8.0	97	65
		8.0~9.0	113	49
		9.0~9.5	130	32
7.5~8.0	18	8.0~9.0	113	49
		9.0~9.5	130	32
8.0~8.5	18	8.5~9.0	113	49
		9.0~9.5	130	32
8.5~10.0	36	$H_2>H_1$	101	43

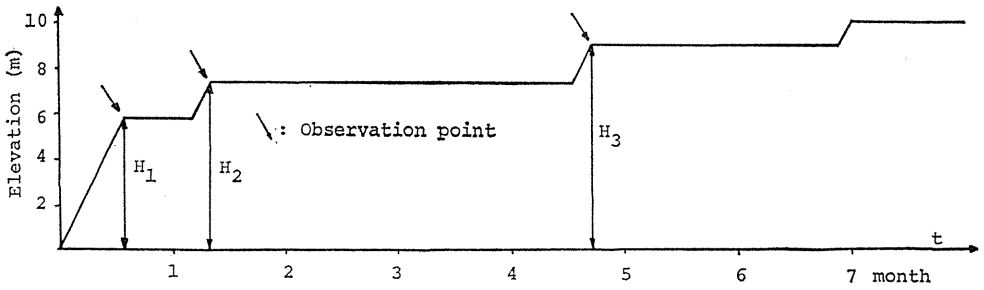

Fig. 3. 15. A typical construction process.

Table 3. 4. Risk ratio

$H=50$ cm	$H=25$ cm	$H=10$ cm	$H=1$ cm
1	0.3	0.05	0.0005

to this figure, for instance.

Incidentally, to decrease the observation error ΔH consequently brings the effect to reduce the risk evaluated in terms of $E[\tilde{P}_F]$ in Eq. (3.36). Taking $\Delta H=50cm$ as the base value of 1, the risk ratios are tabulated in Table 3. 4. The highly precise measurement with $\Delta H=1cm$, if it is possible, can bring the effect to reduce the risk up to the order of 10^{-4} compared with the case of $\Delta H=50cm$. But from a technical viewpoint, such a precise measurement will hardly be expected in practical failure prediction techniques now in use. It should be noted, however, that the optimal design codes do not change in engineering sense in all cases of $\Delta H=25cm$. In other words, the error $\Delta H=25cm$ can be said allowable and this is very convenient for practical failure prediction techniques, since such a value corresponds to the accuracy of actual execution.

4. Dyamic Design Procedure of Excavation

In this chapter, the "Dynamic Design Procedure" proposed in the previous chapter is applied to the excavation works (Matsuo and Kawamura, 1980).

The procedure of design is shown in Fig. 4. 1.

Each procedure is outlined by turns:

(1) The statistical properties of soil parameters of a ground are investigated by soil exploration and tests. (2) The earth pressure acting on the earth retaining structure such as a steel sheet pile wall, a steel pipe sheet pile wall and a retaining wall is computed. (3) The concept of the probability of failure is taken into design to evaluate the degree of safety of the construction field. The analytical errors of the design method which were applied to calculation of the probability of faliure is examined. As was explained in the previos chapter, the analytical error is the error which is caused by various idealization and simplification in the design method. Since the analytical error influences on the magnitude of the probability of failure, it has to be taken into the design as the probability distribution function. In addition, the optimal probability of failure determined in design is usually small in the general engineering problems and therefore not only the distribution but the magnitude itself of the analytical error have to be examined since the large analytical error gives the wrong probability of failure and misleads the optimal decision making. (4) The probability of failure can be computed from the results of (1), (2) and (3). (5) The utility, the cost function in the present study, is defined as the function of the probability of failure. (6) The optimal solution, the optimal action in other words, in the problem of selecting the type of the earth retaining structure and the location of the struts is determined based on

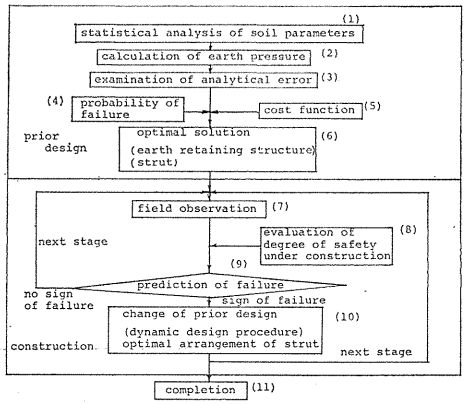

Fig. 4. 1. Procedure of design.

the criterion of evaluation used in design.

In this chapter, the procedurer from (1) to (6) are called the "prior design".

On the other hand, the excavation works will start aiming at the optimal solution obtained in the prior design. At that time, (7) the field observation is carried out during construction in order to evaluate the safety in a construction field and utilize for judgement on necessity of change of the prior design. (8) For this purpose, the method which can quantitatively evaluate the degree of safety under construction is needed. (9) The construction is progressed in examining the safety and whether the failure is going to come or not/is judged by the method (8). (10) If the failure is predicted, the design parameters adopted in the prior design are modified by using the results of observation and the new optimal solution to prevent the actual failure is found. This procedure is repeated during construction and the previous optimal solution is always modified at each time. The previous design is changed like this by new information to make it always optimal. In this chapter, the optimal arrangement of the struts (i. e. number and location of the struts) is decided by the "Dynamic Design Procedtre". (11) Thus the construction is completed safely and economically.

4. 1. Prior-Design

4. 1. 1. Examination of Conventional Design Method

The result of the reliability-based design is strogly influenced by the accuracy of the equations used in design by which the mechanical behavior of a ground and an earth retaining structure are expressed. In this paragraph, a few general design methods are examined from the view point of the analytical error.

(1) Design Methods and Actual Data Examined

The accuracy of a few design methods to calculate the maximum bending moment acting on the earth retaining structure is investigated by many actual data measured in the fields. The simple beam method, the continuous beam method and the approximate method of elasto-plastic solution by Yamagata (1969), all of which are commonly used in the engineering practice, are taken up here.

The maximum bending moment of the earth retaining structure is taken as the factor of examining the design methods, as stated above. The reason is given in the following. The safety of the construction field depends on the safety of the whole system which is composed of the retaining structure, the struts, the wales and other members. But in the general design, the safety of the struts and wales is taken at the higher level than that of the earth retaining structure and therefore it is reasonable to consider that safety of the construction field is equivalent to the safety of the earth retaining structure, which is directly dominated by the maximum bending moment on it.

Rankine earth pressure is applied as the external force on the earth retaining structure. The reason is shown as follows. The earth pressure distributions of the trapezoidal or triangle shape proposed by Terzaghi-Peck (1967) and Tschebotarioff (1951) which were mainly based on the measured results of reaction of the struts have been often used in the practical design. But recently the measuring technique of the earth pressure has been highly improved to make it possible with high accuracy to directly measure the earth pressure on the retaining structure by using the earth pressure gauges and many data have been obtained (Kotoda and

Mori, 1974). According to some research works of examining the earth pressure distribution by these data, Rankine's equation gives the better approximation as compared with other methods (Kotoda and Mori, 1974).

The data associated with the maximum bending moment of the steel sheet pile walls and the steel pipe sheet pile walls which were actually measured in the fields of excavation works of cohesive grounds are used for the later examination of the analytical error. The scales of these construction fields were generally large as shown in Table 4. 1. The avarage number of the struts were five and the maximum bending moment was measured at each cutting stage along with progress of excavation.

Table 4. 1. Construction fields used for examination of design methods.

name of field	retaining structure	state of ground		depth (m)	number of struts
		mean of c_u (kN/m^2)	mean of γ_t ($\times 10^3$kg/m^3)		
No. 1	steel sheet pile	49.0	1.80	11.7	5
No. 2		34.3	1.60	10.0	5
No. 3		50.0	1.72	9.4	3
No. 4		41.2	1.62	16.8	3
No. 5		41.8	1.78	10.4	5
No. 6		47.0	1.66	14.0	4
No. 7	steel pipe sheet pile	44.0	1.80	26.0	5
No. 8		38.0	1.65	25.2	6

(2) Analytical Error on Calculation of the Maximum Bending Moment

The examples of the frequency distribution of the analytical errors on the maximum bending moment calculated by the simple method, the continuos beam method and Yamagata's method are shown in Fig. 4. 2 (a), (b) and (c), respectively. The horizontal axis shows the analytical error e which is defined by the next equation:

$$e=\frac{M_c-M_0}{M_0} \tag{4.1}$$

where M_o denotes the measured maximum bending moment in the excavation fields of cohesive ground and M_c the calculated one by each method under application of Rankine earth pressure which is obtained by the following procedure. Soil parameters such as the undrained strength c_u and the unit weight γ_t are firstly expressed by the probabilistic models according to the results of soil exploration and test. The random variables c_u and γ_t are generally approximated well by the normal distribution as was shown in Chapter 2. Thus the expected value $E[p]$ of Rankine earth pressure is computed as follows:

$$E[p]=\int_{C_u}\int_{\Gamma_t} p(c_u,\gamma_t)f(c_u)f(\gamma_t)\,dc_u d\gamma_t \tag{4.2}$$

where $p(c_u, \gamma_t)$ denotes Rankine earth pressure, C_u and Γ_t the sample spaces of

the random variables c_u and γ_t, respectively and $f(c_u)$ and $f(\gamma_t)$ the probability density functions of c_u and γ_t, respectively.

The dotted lines in Fig. 4.2 show the theoretical probability distributions of the analytical error e which are obtained by χ^2-test on goodness of fit. It is firstly noted that the total width of scatterness of e is much the same in each method. Secondly, both distribution of e of the simple beam and the continuous beam methods can be approximated by the normal distribution and the standard deviation σ is not so different. The logarithmic normal distribution seems to fit to the data better than the normal distribution, but it makes the calculation of the probability of failure more complicated and in addition, as will be seen in the later Fig. 4.3, the case actually adopted in design conforms very well to the normal distribution. On the other hand, e of Yamagata's method is approximated by the uniform distribution as shown in Fig. 4.2. (c) and the value of σ is equal to those of other two methods.

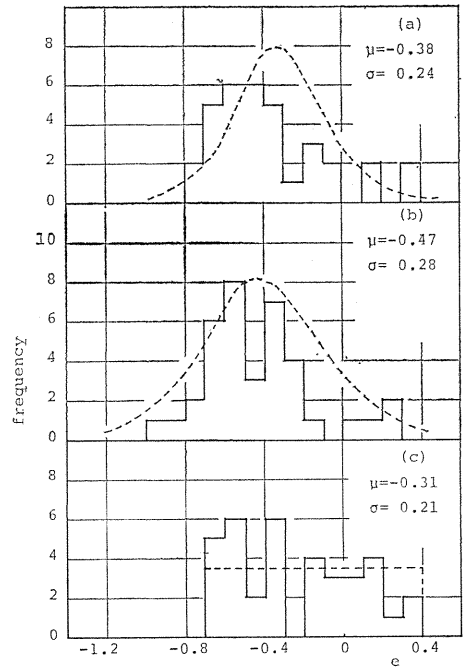

Fig. 4. 2. Analytical error on maximum bending moment.
(a) simple beam method,
(b) continuous beam method,
(c) Yamagata's method.

From these results, the simple beam method is taken in this study for simplicity of calculation of the probability of failure.

(3) Examination of Earth Pressure Distribution at Open Side

The earth pressure below the bottom of the cut at the open side has been assumed to be equal to Rankine passive earth pressure, but there are opinions indicating that the passive earth pressure at the open side does not simultaneously occur with the active earth pressure at the back side of the earth retaining structure because the larger deformation in soil is required to reach the passive state than the active state of the plastic equalibrium. In addition, the negative value of the mean of in Fig. 4.2 (a) suggests the possibility that the smaller pressure than Rankine passive earth pressure is actually mobilized at the open side. From this point of view, the analytical error of the simple beam method is examined again by using the modified earth pressure distribution whose shape is a polygon of (p_p/α) at the base as shown in Fig. 4.3 (a), where α denotes the reduction rate from the passive earth pressure and p_p the intensity of the passive earth pressure at the depth where the moments due to the active and the passive earth pressures at both sides of the earth retaining structure are balanced.

As a result of calculation, it became evident that e corresponding to various values of α conforms to the normal distribution whose parameters μ and σ are given in Table 4.2. The frequency distribution for $\alpha=1.4$ is shown in Eig. 4.3 (b)

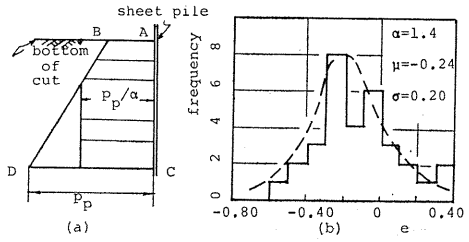

Fig. 4. 3. (a) Modified earth pressure below bottom of cut at open side.
(b) Typical probability distribution on analytical error.

Table 4. 2. Parameters of probability distribution of analytical error.

α	μ	σ
1.0	−0.38	0.24
1.2	−0.31	0.22
1.4	−0.24	0.20
1.6	−0.16	0.22
1.8	−0.12	0.28
2.0	−0.05	0.74
2.2	−0.04	1.32
2.4	−0.01	1.89

as one example and the case of $\alpha=1$ corresponds to Fig. 4.2 (a). As can be seen from Table 4.2, μ approaches zero monotonously with increase of α and σ decreases once to the minimum value but increases in the range of $\alpha\geq 1.6$. The smaller σ is, the better from the view point of accuracy of the reliability-based design and therefore it is desirable to select the design method of having the small σ. Thus the earth pressure distribution modified by $\alpha=1.4$ is used in the later calculation.

4. 1. 2. Probability of Failure of Construction Field

The probability of failure of the earth retaining structure due to the bending moment is defined as follows;

$$P_F=\text{Prob. } (F_s\leq 1) \tag{4.3}$$

$$F_s=\frac{M_a}{M_m} \tag{4.4}$$

where F_s denotes the safety index, M_a the allowable bending moment and M_m the maximum bending moment calculated by the simple beam method. Such the definition of failure as Eqs. (4.3) and (4.4) is common for the structure. M_m is the function of c_u, γ_t and e which are expressed by the normal distributions and therefore M_m also conforms approximately to the normal distribution with the following expected value $E[M_m]$ and variance $V[M_m]$:

$$\left.\begin{aligned}E[M_m]=\int_{\theta_{cu}}\int_{\theta_{\gamma t}}\int_{\theta_e}\{\sum_{G_{cu}}\sum_{G_{\gamma t}}\sum_{G_e} m(c_u,\gamma_t,e)g(c_u|\theta_{cu})g(\gamma_t|\theta_{\gamma t})g(e|\theta_e)\}\\ \times\xi(\theta_{cu})\xi(\theta_{\gamma t})\xi(\theta_e)d\theta_{cu}d\theta_{\gamma t}d\theta_e\end{aligned}\right\} \tag{4.5}$$

$$\left.\begin{aligned}V[M_m]=\int_{\theta_{cu}}\int_{\theta_{\gamma t}}\int_{\theta_e}\{\sum_{G_{cu}}\sum_{G_{\gamma t}}\sum_{G_e}(m(c_u,\gamma_t,e)-E[M_m])^2 g(c_u|\theta_{cu})g(\gamma_t|\theta_{\gamma t})\\ \times g(e|\theta_e)\}\xi(\theta_{cu})\xi(\theta_{\gamma t})\xi(\theta_e)d\theta_{cu}d\theta_{\gamma t}d\theta_e\end{aligned}\right\} \tag{4.6}$$

where θ_{cu}, $\theta_{\gamma t}$ and θ_e are the parameters (mean and variance) of the population of each c_u, γ_t and e and their probability density function $\xi(\theta_{cu})$, $\xi(\theta_{\gamma t})$ and $\xi(\theta_e)$,

respectively. $m(c_u, \gamma_t, e)$ is the maximum bending moment of the earth retaining structure for the set of (c_u, γ_t, e) mobilized from each $g(c_u|\theta_{cu})$, $g(\gamma_t|\theta_{\gamma t})$ and $g(e|\theta_e)$ which is the probability distribution of each c_u, γ_t and e under the parameters of θ_{cu}, $\theta_{\gamma t}$ and θ_e, respectively. Θ_{cu}, $\Theta_{\gamma t}$, Θ_e, G_{cu}, $G_{\gamma t}$ and G_e are the probability spaces of θ_{cu}, $\theta_{\gamma t}$, θ_e, $g(c_u|\theta_{cu})$, $g(\gamma_t|\theta_{\gamma t})$ and $g(e|\theta_e)$, respectively.

The cost function which can estimate the alternatives of the prior-design is the same to Eq. (3.8).

4. 1. 3. Numerical Examples

The optimal material and type of the earth retaining structure, and the optimal number and location of the struts are determined here as the prior-design. The obtained restlts are compared with the actual cases of excavation works which were completed successfully.

Table 4. 3. Type of steel sheet pile with section modulus W and yield stress σ_y.

type	W (cm³)	σ_y ($\times 10^2$kN/m²)
SP-Ⅱ	869.0	3 000
SP-Ⅲ	1 310.0	4 000
SP-Ⅳ	2 060.0	4 000
SP-Ⅴ	3 150.0	4 000
SP-Z32	3 190.0	4 000

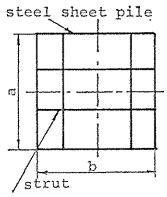

(unit;m)

model	A	B	C	D
a	9.0	12.0	12.5	18.0
b	9.0	12.0	13.0	27.0
depth	10.0	12.0	14.0	18.0

Fig. 4. 4. Excavation field models.

Some numerical examples for the very common-steel sheet piles in Table 4.3 are shown here. Four cases of excavation of Fig. 4.4 are considered as the field models and corresponding to each case, over four cases of the strut arrangement are examined as shown in Fig. 4.5 and Table 4.4. With reference to the past actual results, the first strut s_0 near the ground surface is assumed at first and

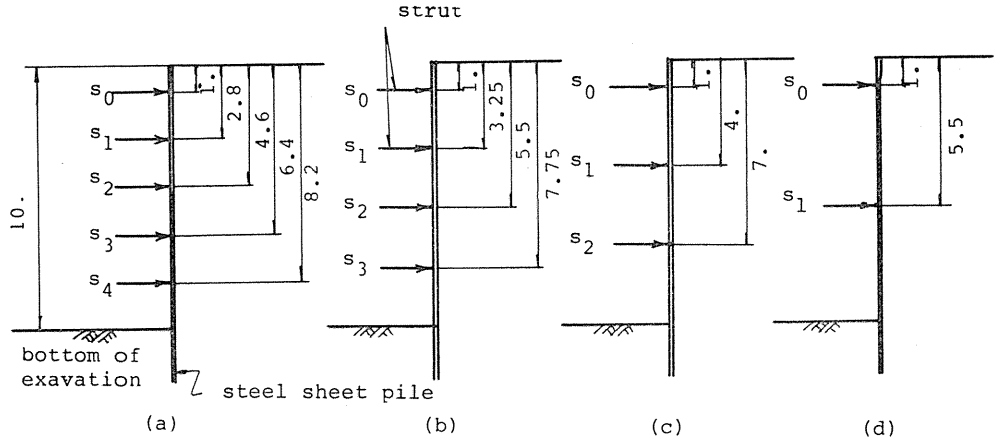

Fig. 4. 5. Arrangement of struts in model (A). (unit; m)

Table 4. 4. Arrangement of struts in each model. (unit; (m))

model and depth	number of struts	s_0	s_1	s_2	s_3	s_4	s_5	s_6
(B) 12 m	6	1.5	3.3	5.1	6.9	8.7	10.5	
	5	1.5	3.6	5.7	7.8	10.0		
	4	1.5	4.2	6.8	9.8			
	3	1.5	5.0	8.5				
	2	1.5	6.8					
(C) 14 m	6	2.0	3.5	5.5	7.5	9.5	11.5	
	5	2.0	4.0	6.5	9.0	11.5		
	4	2.0	5.0	8.0	11.0			
	3	2.0	6.0	10.0				
	2	2.0	8.0					
(D) 18 m	7	2.0	4.5	6.7	8.9	11.1	13.3	15.8
	6	2.0	5.0	8.0	11.0	13.0	16.0	
	5	2.0	5.0	8.5	12.0	15.5		
	4	2.0	6.0	10.0	14.0			
	3	2.0	8.0	13.0				

the depth under s_0 is divided at nearly equal intervals as the location of each. strut. Except the case of the lowest strut, the bottom of each cutting stage is assumed at 0.5 m below the appointed location of the strut in that stage as usually done in the general excavation works. The common cohesive ground of which c_u and γ_t have the means of 34.3 kN/m^2 and $1.6\times10\ kg/m^3$ and the coefficients of variation of 0.2 and 0.03, respctively, is assumed as the field condition. Based on the recent actual results, each cost in Eq. (3.8) is summed up for each model of Fig. 4.4.

The optimal solutions for all cases are summarized in Table 4.5 with the corresponding probability of failure. It is noted that the obtained optimal solutions

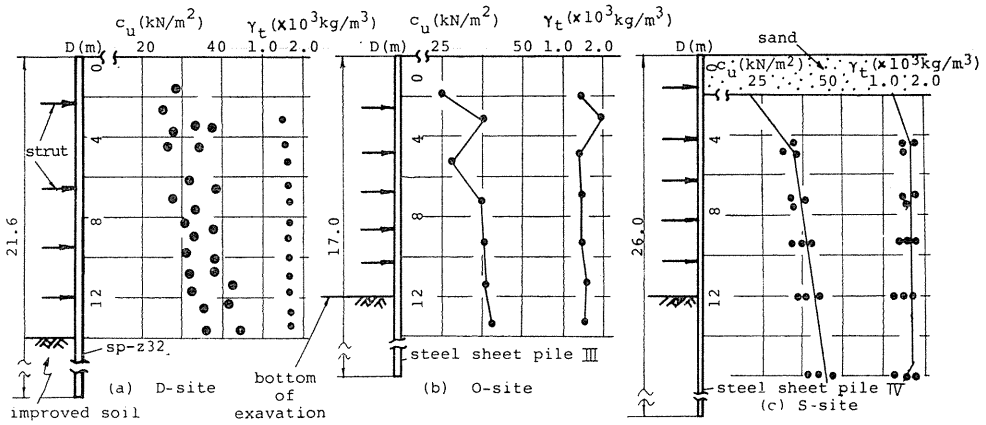

Fig. 4. 6. Ground conditions and location of struts of actual cases.

Table 4. 5. Optimal solutions.

model	depth (m)	type of steel sheet pile	number of struts	$(P_F)_{opt}$ (%)
A	10	SP-Ⅳ	4	5.8
B	12	SP-Ⅴ	4	16.5
C	14	SP-Ⅴ	5	25.5
D	18	SP-Ⅴ	6	43.0

indicate the selection of common sense concerning the type of the earth retaining structure and the vertical interval of the struts.

In order to examine usefulness of the analytical method a little more in detail, the optimal solutions in Table 4.5 are compared with the actually completed excavation works which had the similar conditions to the numerical examples. The ground conditions and the location of the struts of the actual cases compared in this section are shown in Fig. 4.6. Cutting was carried out up to $12\,m$ or $14\,m$ deep. The undrained strength and the unit weight of these cohesive grounds were about $34.0 kN/m^2$ and $1.6\times 10 kg/m^3$, respectively, as shown in the figure. The vertical intervals of the struts were unequal, but not so different. If the depth of excavation, the type and arrangement of struts and wales, the cost of earth works and the surrounding conditions of the construction field do not change, the optimal solution for the type of earth retaining structure and the number of struts determined by Eq. (3.8) is not influenced by the width of excavation. The actual cases compared here have the different width from the numerical examples, but the above stated conditions are not so different from those of the numerical examples and therefore it is not unreasonable to compare them with model (B) and (C) in the numerical examples. The results are given in Table 4.6. The type of sheet pile and the number of struts adopted in the actual cases are given in the left column, with the corresponding probability of failure $(P_F)_1$ in each case which is computed for the arrangement of struts in Fig. 4.6. The central column shows the analytical results from Table 4.5. Incidentally, the right column gives the optimal number of struts and the probability of failure $(P_F)_2$ which are analytically obtained when the same type of sheet pile to the actual case is taken in calculation.

Table 4. 6. Comparison with actual cases.

actual case						optimal solution				optimal number of struts	
site	depth (m)	width (m)	number of struts	type of steel sheet pile	$(P_F)_1$ (%)	model	number of struts	type of steel sheet pile	$(P_F)_{opt}$ (%)	number of struts	$(P_F)_2$ (%)
D	14.0	41.0	4	SP-Z 32	26.0	C	5	SP-Ⅴ	25.5	5	23.4
O	12.0	8.5	5	SP-Ⅲ	18.5	B	4	SP-Ⅴ	16.5	6	17.2
S	12.0	19.0	5	SP-Ⅵ	16.8	B	4	SP-Ⅴ	16.5	6	15.7

It can be seen from comparison of the left and the central columns that the optimal solution calculated by the proposed method gives a little safer side than the actual result. That is, the optimal solution in calculation requires the type of

sheet pile of the higher rigidity and the smaller probability of failure than the actual case. Similarly, according to comparison of the left and the right columns, the latter needs one more strut than the formar and consequently, the probability of failure decreases a little. But generally speaking from these results, the proposed method can give the very close solution to the actual design which must be determined on the basis of ripe experience of many engineers and thus this can be said useful in decision making in the prior design.

Finally the following point should be discussed. The probability of failure in Table 4.6 seems too large and unreal. The true probability of failure in the actual construction field might be much smaller. Such a large probability in calculation is mainly caused by two points. One is the use of the simple beam method in which the bearing effect of the struts except the lowest one which have been already built is neglected. The other cause is the assumption of the simplest modeling of the ground (Matsuo, 1976). If the more exact model is applid, the very small probability of failure which may corresponds to the reality is obtained, but much complicated procedure and time are needed. The probability of failure is necessary for decision making, but the magnitude itself is unnecessary for it and in addition, it was ascertained that the influence of using the simple model on the optimal selection from the the alternatives is very small. It is needless to say that the simpler the design method is, the better it is if the result of decision making does not change.

4. 2. Prediton of Failure by Field Observation

The optimal solution of the prior design is determined, as shown in the previous section, by using information offered before the construction starts. This optimal solution, however, still have various uncertainty due to idealization and simplification in test and design. In addition, since the probability of failure is by no means zero even if it is the optimal solution, the construction field has always the possibility of failure. The excuse that the failure has unfortunately occured in spite of making the prior design optimal cannot be permitted in practice, so that the safety during construction has to be always checked and if the sign of failure appears, the prior design should be positively changed during construction in order to prevent the coming actual failure, as shown later. For this purpose, it is necessary to find the method to predict the forthcoming failure and quickly control the construction. (Peck, 1969; Matsuo and Kawamura, 1980).

4. 2. 1. Degree of Safety during Construction

Let us examine on the degree of safety in the field through construction. If the failure occurs at the final stage of excavation, the loss may become large than the loss due to the small-sized failure in the early stage of excavation. So it is unreasonable to decrease the degree of safety with the progress of excavation. In other words, from the mechanical and economical view point, the degree of safety of the construction field should be kept at the equivalent level at least or gradually raised little by little during construction. It may be allowed to consider that this principle has been held in the recent large-sized excavation works completed successfully, since they have been performed under accumulation of the wealth of knowledge and the ripe experience of many engineers and therefore it is natural to conclude that they were not unduly dangerous and unduly uneconomical. This view point forms the foundation of the proposed method in the next section.

Fig. 4. 7 shows one example of the recent large-sized excavation works which was successfully completed up to 10.4 m deep in the poor ground whose average undrained shear strength and unit weight were 41.2 KN/m^2 and 1.68×10^3 kg/m^3, respectively. Fig. 4. 7 (a) gives the rate of change of the deflection angle of the steel sheet pile in each cutting stage which directly corresponds to the bending

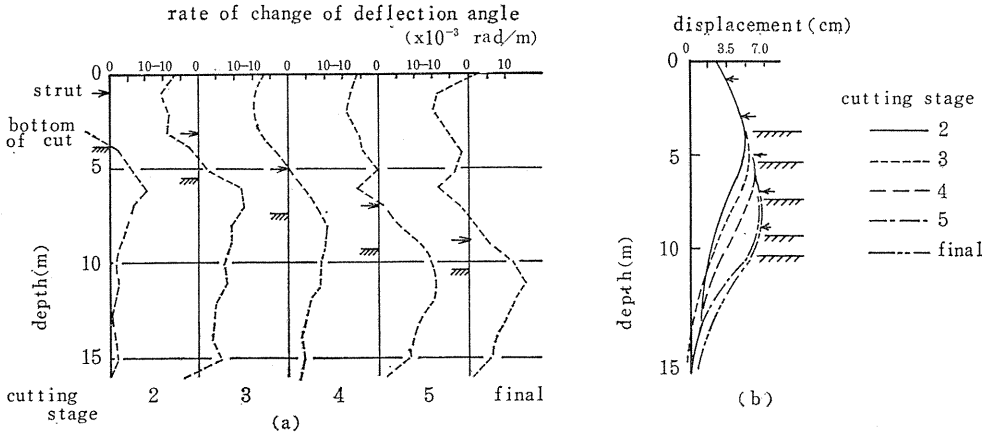

Fig. 4. 7. One example of excavation work. (No. 5. in Table 4. 7.)
(a) rate of change of deflection angle,
(b) horizontal displacement.

moment of the sheet pile. Fig. 4. 7 (b) shows the horizontal displacement of the same sheet pile in each cutting stage. It can be seen from Fig. 4. 7 (a) that the maximum bending moment is kept nearly constant up to the fourth cutting stage and although a little increase is seen in the fifth stage, it rather somewhat decreases in the final stage. Similarly from Fig. 4. 7 (b), the maximum horizontal displacement is constantly about 6 cm up to the fourth stage and becomes 7 cm in the next stage, but does not increase until the end of final excavation. These results suggest that the engineers carefully controlled the cutting works to keep the equal degree of safety at least through construction.

Even if in the construction fields where the bending moment and the horizontal displacement increased a little with the progress of excavation, the engineers were convinced yet that the degree of safety did not decrease as a whole, because they took the more cautious attitude by increasing the checkborings and the frequency of field observation and sometimes by using the more rigid struts and wales.

4. 2. 2. Behavior of Earth Retaining Structure

In this section, the behavior of an earth retaining structure is taken as the index to estimate the degree of safety of a work according to the following reasons. In the general design philosophy, the safety of the struts and the wales is taken at the higher level than that of the earth retaining structure and therefore it can be considered that the safety of the construction field is equivalent to the safety of the earth retaining structure.

The shape of deformation of the earth retaining structure is similar to that

of deflection of the simple beam which is supported at both the point of the first strut near the ground surface and the point under the bottom of the cut where the bending moment of the retaining structure becomes zero (Bjerrum and Eide, 1956). Therefore if the distribution of the earth pressure acting on the retaining structure is approximated by a triangle or a rectangle, the deformation in the elastic zone of the retaining structure is reasonably assumed as follows:

$$\frac{yEI}{p'L^4}=Af\left(\frac{l}{L}\right) \tag{4.7}$$

where, as shown in Fig. 4. 8, y denotes the lateral displacement of the earth retaining structure at an optional point in each cutting stage, l the depth of the same point from the ground surface, L the span length of the earth retaining structure as a simple beam, p' the intensity of the lateral earth pressure at the point of the zero bending moment under the bottom of the cut, EI the bending rigidity of the earth retaining structure and $f(l/L)$ and A the function of (l/L) and the constant, respectively, both of which depend on the distribution of earth pressure.

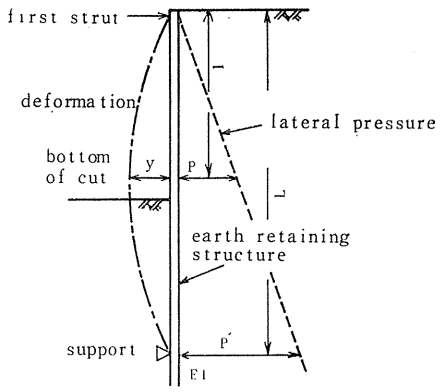

Fig. 4. 8. Deformation of earth retaining structure.

According to many observed results, the maximum displacement y_{max} in each cutting stage appeared near the bottom of the cut and therefore the following equation can be obtained by substituting $(l/L) \fallingdotseq$ constant into Eq. (4. 1) because of $p'=Bp$ in which B becomes a constant if the distribution of earth pressure is assumed a triangle:

$$\frac{y_{max}EI}{pl^4}=\beta \tag{4.8}$$

where p is the intensity of the lateral earth pressure at the bottom of the cut in each cutting stage and β is a constant.

Fig. 4. 9 (a) ~ (c) show the observed results associated with the steel sheet pile, the steel pipe sheet pile and the reinforced concrete diaphragm wall in fifteen actual constrtction fields in Japan. No. 1, No. 2 etc. are the convenient names of the fields whose scales of excavation and the state of the grounds are given in Table 4.7. In those figures, the logarithmic values of $(y_{max}EI)$ and (pl^4) are taken as both axes and the numeral shows the cutting stage and the arrow indicates

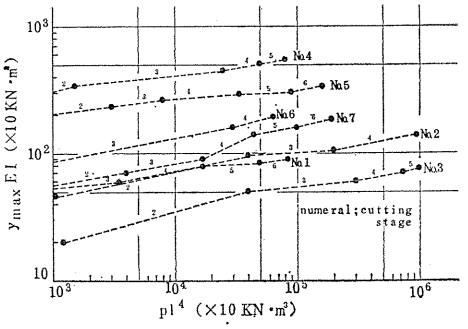

(a) STEEL SHEET PILE

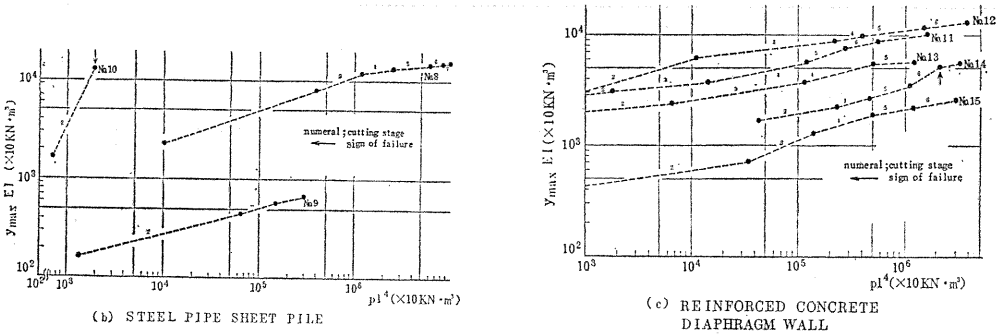

(b) STEEL PIPE SHEET PILE

(c) REINFORCED CONCRETE DIAPHRAGM WALL

Fig. 4. 9. $\log pl^4 \sim \log y_{max}EI$.

Table 4. 7. Constrection fields.

site	type of retaining structure	cutting depth (m)	mean undrained shearing strength (kN/m^2)	mean unit weight (t/m^3)	depth of embedment of retaining structure (m)	number of struts
No. 1	steel sheet pile	10.0	34.3	1.60	2.4	5
No. 2		16.8	41.2	1.62	11.2	3
No. 3		14.0	47.0	1.66	10.0	4
No. 4		13.0	32.3	1.61	6.0	4
No. 5		10.4	41.2	1.68	6.2	5
No. 6		9.4	50.0	1.70	9.6	3
No. 7		11.7	49.0	1.80	11.1	5
No. 8	steel pipe sheet pile	26.0	44.1	1.80	21.5	5
No. 9		14.0	32.3	1.65	7.0	3
No. 10*		4.8	24.5	1.45	40.0	1
No. 11	reinforced concrete diaphragm wall	19.1	44.1	1.65	8.4	6
No. 12		21.0	39.2	1.55	23.0	4
No. 13		15.8	41.2	1.70	—	4
No. 14*		22.0	42.0	1.55	20.5	6
No. 15		18.0	73.5	1.80	—	5

* sign of failure was observed

the moment when the sign of failure appeared.

Let us first see the cases with no arrow in Fig. 4. 9 which were safely completed with no trouble. In these cases, as expected from Eq. (4. 8), $\log pl^4$ and $\log y_{max}EI$ has the linear relation with a nearly constant or a little decreasing gradient in each case throughout the construction. This tendency is the same

irrespective of the type of the earth retaining structure.

On the other hand, the case No. 14 in which the failure was once predicted has a little different tendency. In No. 14-field, when the excavation reached 16.9 m in depth as the sixth cutting stage, the stress of the reinforcement became $27\times 10^4\ KN/m^2$ which exceeded the yield value of the reinforcement of $24\times 10^4\ KN/m^2$, so that the excavation was once stopped and the sixth strut was built at 16.5 m in depth.

It should be noted in Fig. 4. 9 (c) that the gradient of the ($\log pl^4 \sim \log y_{max} EI$) relation obviously increases during the sixth cutting stage as compared the gradient up to the fifth cutting stage. The No. 10-field in Fig 4. 9 (b) has the quite similar tendency.

The above stated facts show the usefulness of plotting such as Fig. 4. 9 in order to roughly check the safety of the excavation field, but it is not accurate enough for engineering practice to quantitatively evaluate the degree of safety because the somewhat high gradient is sometimes observed even at the actually safe condition at the shallow excavation stage such as the third cutting stage of No. 15 in Fig. 4. 9 (c), for instance. So the following arrangement is proposed.

4. 2. 3. Method of Prediction of Failure

It is very useful if the safety of the earth retaining structure can be quantitatively estimated by the magnitude of the gradient of the relationship between pl^4 and $y_{max}EI$ in Eq. (4.8). In this case, it is natural to consider that the critical gradient which gives the dangerous condition is related with the cutting depth from a ground surface. For example, the relatively larger critical gradient may be allowed in the early stage of excavation as compared in the deep cutting stage.

The logarithmic value of β in Eq. (4.8) calculated by using the same data to those used in Fig. 4. 9 is plotted against the cutting depth D as shown in Fig. 4. 10 (a), (b) and (c) which are clasified by the type of the earth retaining structure. In this case, the values of y_{max} and p at the beginning and the end of each cutting stage are applied to obtain β. On the other hand, the depth at the beginning of the same cutting stage is adopted as D, because it is considered more useful for the prediction of failure in that cutting stage.

If Eq. (4.8) correctly expresses the real behavior of the construction field, β must be kept constant. But it is evident from Fig. 4. 10 that β generally decreases with the progress of excavation and this tendency does not change in all types of the earth retaining structures. Such a gap is caused by the difference between the reality and the calculation method by Eq. (4.8) which has some simplifacation. For example, Eq. (4.8) is obtained by assuming the earth retaining structure as the simple beam with two end supports and therefore the effect of the intermediate struts is neglected in Eq. (4.8) although there exists actually. Turning this situation over, however, it should be especially noted that if the same degree of magnitude of β to that in the shallow excavation stage is produced also in the deeper cutting stage in spite of existence of the effect of the intermediate struts, this must mean that the construction filed is now in the extreme dangerous condition or has already failed.

According to the experimental facts of many practicians described in the previous section, it should be considered that the decline of β with D such as in Fig. 4. 10 can just keep the degree of safety of the construction field in nearly constant at least. In other words, each line of Fig. 4. 10 is interpreted to show the own

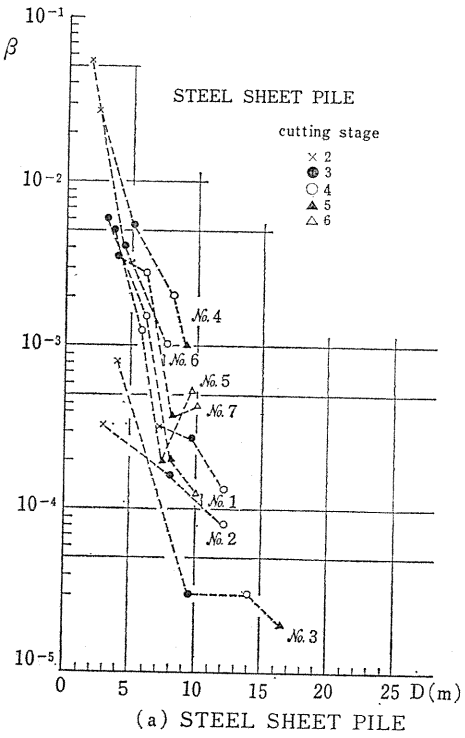

(a) STEEL SHEET PILE

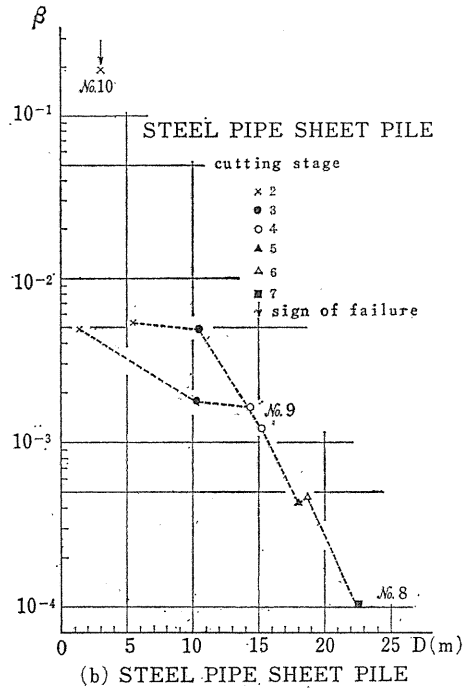

(b) STEEL PIPE SHEET PILE

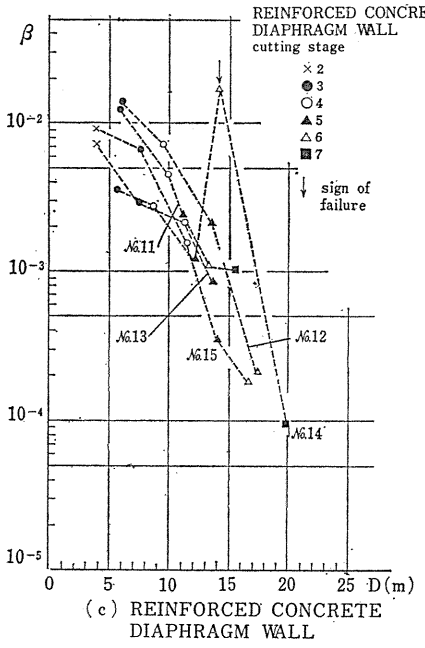

(c) REINFORCED CONCRETE DIAPHRAGM WALL

Fig. 4. 10. $D \sim \log \beta$.

contour line of the degree of safety of the construction field.

The properties of the observed values of β are investigated in detail from the above stated view point. Since there is no significant difference in the tendency of the relation of β and D due to the types of the earth retaining structures, all data in Fig. 4. 10 are used to examine the characteristics of decline of β. Denoting the values of β in the i-th and the $(i\text{-}1)$-th cutting stages by β_i and β_{i-1}, respectively, β_i is expressed as follows:

$$\beta_i = \alpha_i \beta_{i-1} \tag{4.9}$$

where α_i is the declining factor in the i-th cutting stage. Fig. 4. 11 shows the histogram of the logarithmic value of α_i of the construction fields where the excavations were completed with no trouble. It is obvious from this figure that $\log \alpha_i$ conforms well to the normal distribution in which the dotted line shows the theoretical curve. Specifically to be noted is the fact that $\log \alpha_i$ becomes a negative number with the probability of 86%. This means that $\log \beta$ becomes a monotonously decreasing function against the cutting depth in almost cases completed successfully. In addition, according to Fig. 4. 10, the declining manner of $\log \beta$ is approximately linear to D. In fact, the very high mean, 0.92, of the coefficient of correlation between $\log \beta$ and D was calculated by applying a linear regression analysis to the relation of $\log \beta$ and D in each construction field with no trouble. Therefore, $\log \beta$ can be expressed by the following linear model:

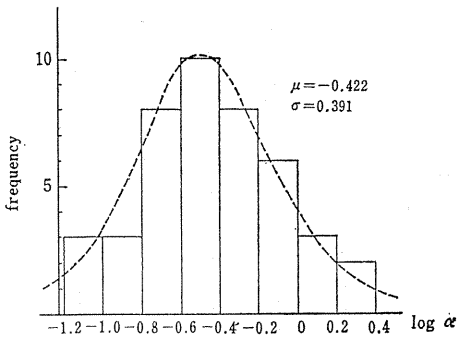

Fig. 4. 11. Histogram of $\log \alpha$.

$$\log \beta = \log a + b D \tag{4.10}$$

where $\log a$ and b are the parameters of the linear function.

The gradient b in Eq. (4.10) is very important to obtain the good contour line representing the degree of safety of the construction field. Fig. 4. 10 (a) has a little different region of the plotted points and magnitude of b from those of Fig. 4. 10 (b) and (c), as can be seen in the figures, and therefore the following quantitative examination is separately carried out in two groups. Fig. 4. 12 shows the histograms of b associated with the construction fields which had no trouble. Fig. 4. 12 (a) is the result of the steel sheet piles and Fig. 4. 12 (b) is concerned with the reinforced concrete diaphragm walls and the steel pipe sheet piles, where the dotted lines are the theoretical curves of the normal distribution to which the value of b follows well. It is important here that the dissipation of b is very small. Thus the following approximate equations are given to control the displacement of the earth retaining structure and keep the degree of safety nearly constant at least during construction:

$$\log \beta = \log a - 0.236 D \tag{4.10—a}$$

for the steel sheet pile and

$$\log \beta = \log a - 0.120\, D \qquad (4.10\text{—b})$$

for the reinforced concrete diaphragm wall and the steel pipe sheet pile.

Fqs. (4. 10-a) and (4. 10-b) show the contours of the degree of safety as was already discussed. The next very interesting and important problem for engineering practice is to determine the failure criterion line. This is equivalent to determine $\log a_f$ in the following equation:

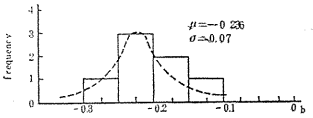

(a) STEEL SHEET PILE

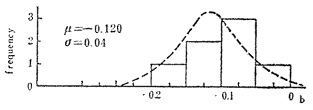

(b) STEET PIPE SHEET PILE
REINFORCED CONCRETE DIAPHRAGM WALL

Fig. 4. 12. Histogram of b.

$$\log \beta_f = \log a_f + b\, D \qquad (4.11)$$

where β_f and a_f are the values of β and a at failure, respectively. Unfortunately (perhaps it should be said "fortunately"), there are only a few cases which actually showed the sign of failure during construction and therefore it is very diffcult to fix the exact failure criterion line. However so long as standing on the inductive view point, the actual results obtained thus far should be considered most important for the present. The equations to be proposed in this meaning are Eqs. (4. 12-a) and (4. 12-b):

$$\log \beta_f = -0.79 - 0.236\, D \qquad (4.12\text{—a})$$

for the steel sheet pile and

$$\log \beta_f = -1.02 - 0.120\, D \qquad (4.12\text{—b})$$

for the reinforced concrete diaphragm wall and the steel pipe sheet pile. These are shown in Fig. 4. 13 by the solid lines which envelop all plotted points of the no-trouble cases of the construction fields. The points corresponding to the cases in which the sign of failure appeared are located obviously beyond the line of Eq. (4. 12)

Eqs. (4. 12-a) and (4. 12-b) become the critical lines for the construction control of the excavation works. But considering that the coefficient of correlation is not equal to one and the gradient b is a random variable although the dissipation is small, it is reasonable to hold the limitation of the safety a little lower than these critical lines for practical use. Incidentally three chain lines below the failure criterion lines indicate the contours which represent 90 %, 80 % and 70 % values of $\log \beta_f$ calculated at the same depth D. These lines may become the guide lines to control the construction at the nearly same level of the degree of safety. Each line will be selected by an engineer based on his experience, self-confidence and engineering judgement and if the value of $\log \beta$ observed during construction exceeds his line, the appropriate countermeasures should be taken very quickly.

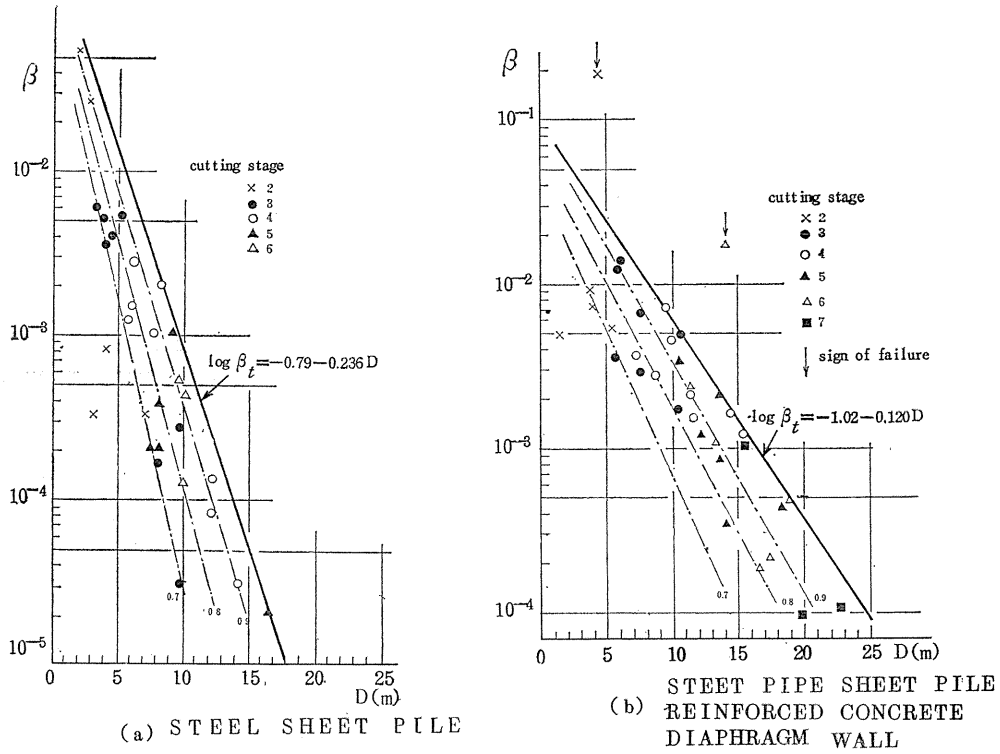

Fig. 4. 13. Diagram for construction control.

4. 3. Modification of Design during Construction

4. 3. 1, Re-formulation of the "Dynamic Design Procedure" for Excavation works

With reference to formulation associated with the embankment problem in chapter 3, the "Dynamic Design Procedure" of the excavation problem is formulated as follows.

The optimal arrangement of struts can be determined by the criterion of minimizing the Bayes' risk (Benjamin and Cornell, 1970; Raiffa and Schlaifer, 1961). Let us firstly consider the probability distribution indicating the degree of reasonable belief of the parameter θ which expresses the state of the earth pressure on the earth retaining structure. Initial belief of θ can be generally given as the probability density function $\xi(\theta)$ which is determined by using the results of soil explorations and past experiences before the excavation begins. The excavation now starts and steadily progresses after building the first strut s_0 near the head of the earth retaining structure. It is assumed in Fig. 4. 14 that the first sign of failure has appeared at the cutting depth of $(a_1 \sim a_1 + \Delta a)$, where Δa denotes the observational error. This situation means that the actually mobilized true safety factor f has become nearly equal to one at that depth. It was already found in the previous chapter that under such a condition, the prior distribution $\xi(\theta)$ given before the excavation can be modified by using the Bayes' theorem as shown in the

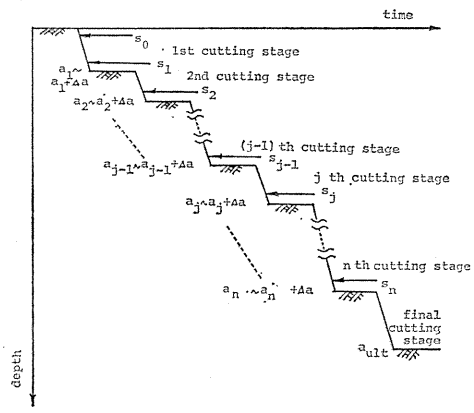

Fig. 4. 14. Illustration of progress of excavation.

following equation;

$$\xi(\theta|a_1,\ s_0)=\frac{\{P_F(\theta,\ a_1+\Delta a|s_0)-P_F(\theta,\ a_1|s_0)\xi(\theta)}{\int\text{numerator}\ d\theta} \tag{4.13}$$

where the left hund $\xi(\theta|a_1,\ s_0)$ means that $\xi(\theta)$ has been modified by the new condition of building s_0 and observing the first sign of failure at $(a_1\sim a_1+\Delta a)$. Since the actual occurrence of failure is not permitted, the strut s_1 is quickly built at that time in the optimal depth selected. Assuming that the state of the earth pressure does not change before and after building the strut s_1, the next equation is given;

$$\xi(\theta|a_1,\ s_1)=\xi(\theta|a_1,\ s_0) \tag{4.14}$$

If the similar procedure is repeated in the successive cutting stage, the next equation can be obtained by recurrence operation of Eq. (4. 13)

$$\xi(\theta|a^j,\ s^{j-1})=\frac{\{P_F(\theta,\ a_j+\Delta a|s^{j-1})-P_F(\theta,\ a_j|s^{j-1})\}\xi(\theta|a^{j-1},\ s^{j-1})}{\int\text{numerator}\ d\theta} \tag{4.15}$$

where a^j and s^{j-1} denote the history of the observed depths of the sign of failure and the corresponding struts, respectively:

$$a^j=\{a_1,\ a_2,\ \cdots,\ a_j\}$$

$$s^{j-1}=\{s_0,\ s_1,\ \cdots,\ s_{j-1}\}$$

The subject is to determine the optimal location of strut s_j^* under the given matrices of a^j and s^{j-1}. The following notation is used to express s_j^*:

$$s_j^*=s_j^*(a^j,\ s^{j-1}),\ j\geq 1 \tag{4.16}$$

which shows that s_j^* is the function of a^j and s^{j-1}. To be optimized for all of j means that the next equations should be sloved:

$$\left.\begin{aligned} s_1^* &= s_1^*(a_1,\ s_0) = s_1^*(a^1,\ s^0) \\ s_2^* &= s_2^*(a_2,\ a_1,\ s_1^*,\ s_0) = s_2^*(a^2,\ s^{1*}) \\ &\vdots \qquad\qquad \vdots \\ s_n^* &= s_n^*(a^n,\ s^{n-1*}) \end{aligned}\right\} \tag{4.17}$$

These optimal solutions of Eq. (4.17) can be obtained with the following manner.

Assuming that the total number of struts which have been built is n except the first strut s_0 (see Fig. 4. 14), the loss function $L(\theta,\ s^n)$ corresponding to the excavation of the appointed final depth a_{ult} which is estimated at the moment of finishing the construction of s_n can be written as follows:

$$L(\theta,\ s^n) = C_C\{1 - P_F(\theta,\ a_{ult}|s^n)\} + C_F \cdot P_F(\theta,\ a_{ult}|s^n) \tag{4.18}$$

where C_C and C_F, the function of n, are the same to those in Eq. (3.8) and $P_F(\theta,\ a_{ult}|s^n)$ shows the probability of failure of the construction field at the moment when the excavation will reach the final depth a_{ult} after building the strut s^n.

Let us next try to predict the loss function when the struts s^{n-1} have been just built based on the observation of a^{n-1} but a_n is not observed yet. This predictive expected value of the loss, ν_n, is given by the following equation;

$$\nu_n = \int_\theta \sum_{A_n} \text{Prob.}(a_n < a < a_n + \Delta a|\theta) \cdot \xi(\theta|a^{n-1},\ s^{n-1}) \cdot L(\theta,\ s^n)\, d\theta \tag{4.19}$$

where A_n and θ are the possible sample spaces of a_n and θ, respectively and Prob. $(a_n < a < a_n + \Delta a|\theta)$ is the probability to find the sign of failure at $(a_n \sim a_n + \Delta a)$ conditioned by the state of earth pressure θ which is given as follows (Matsuo and Asaoka, 1978);

$$\text{Prob.}(a_n < a < a_n + \Delta a) = P_F(\theta,\ a_n + \Delta a|s^{n-1}) - P_R(\theta,\ a_n|s^{n-1}) \tag{4.20}$$

Substituting Eq. (4.20) into Eq. (4.19) and applying Eq. (4.15) to it, the next equation is given:

$$\nu_n \propto \sum_{A_n} \int_\theta \xi(\theta|a^n,\ s^{n-1}) \cdot L(\theta,\ s^n)\, d\theta \tag{4.21}$$

where the proportional constant corresponds to the denominator of Eq. (4.15) which has no relation with s_n. It must be noted here that s_n is the function of a^n an s^{n-1}. Since a^{n-1} and s^{n-1} have been already known, s^n to minimize the expected value ν_n can be determined by the next equation which is the function of a_n.

$$\min \nu_n \propto \sum_{A_n} \min_{S_n} \int_\theta \xi(\theta|a^n,\ s^{n-1}) \cdot L(\theta,\ s^n)\, d\theta \tag{4.22}$$

where S_n is the possible sample space of s_n. Eq. (4.22) means to specify the optimal strut s_n^* in the given region of $a_n \in A_n$ and thus s_n^* has been determined as follows;

$$s_n^* = s_n^*(a^n, s^{n-1}) \tag{4.23}$$

Similarly the loss of Eq. (4.18) can be predicted also at the stage where a^{n-2} and s^{n-2} have been already known but a_{n-1}, a_n, s_{n-1} and s_n are unknown yet. Denoting this expected value by ν_{n-1}, ν_{n-1} is obviously expressed as follows;

$$\nu_{n-1}=\int_\theta \sum_{\Delta n-1} \text{Prob.}(a_{n-1}<a<a_{n-1}+\Delta a|\theta)\cdot\hat{\xi}(\theta|a^{n-2},\ s^{n-2})\cdot\nu_n d\theta \qquad (4.24)$$

which is the same form to Eq. (4.19). Therefore it is easily understood that Eq. (4.25) of the same form to Eq. (4.22) can be used and the optimal strut s^*_{n-1} is determined as shown in Eq. (4.25);

$$\min \nu_{n-1} \propto \sum_{\Delta n-1} \min_{S n-1} \int_\theta \hat{\xi}(\theta|a^{n-1},\ s^{n-2})\cdot\nu_n d\theta \qquad (4.25)$$

$$s^*_{n-1}=s^*_{n-1}(a^{n-1},\ s^{n-2}) \qquad (4.26)$$

If the quite similar calculations are recurrently carried out by going back to the first cutting stage, the series of the optimal locations of struct s^*_j which minimize the predictive value of the loss at the finishing stage of excavation can be obtained in the order from the upper part of Eq. (4.27)

$$\begin{aligned} s^*_n &= s^*_n(a^n,\ s^{n-1}) \\ s^*_{n-1} &= s^*_{n-1}(a^{n-1},\ s^{n-2}) \\ &\vdots \quad\quad \vdots \\ s^*_1 &= s^*_1(a_1,\ s_0) \end{aligned} \qquad (4.27)$$

Substituting the actually observed values of a_j $(j=1, 2, \ldots, n)$ into Eq. (4.27) and following the solutions in the order of $j=1\rightarrow n$, it is just the path of the optimal construction of struts.

4. 3. 2. Numerical Examples

The method to decide the optimal arrangement of the struts was formulated, but it is too late to begin the calculation of the Beyes' risk after the sign of failure has been found during construction since the countermeasure has to be quickly taken at that time. So it is indispensable for practical use to calculate various possible cases and represent the results in the table or the figure in advance of excavation, because the engineers can find at once their optimal action from it when they see the indication of failure during construction. One example of the table which is made for this purpose is Table 4. 8.

The conditions used in the numerical examples in Table 4. 8 are as follows: The final depth of excavation a_{ult} is $10\,m$. Since Δa is considered about $(0.5\sim1)m$ practically, $\Delta a=1.0\,m$ is assumed here. As c_u, γ_t and e, the same values to those which were used in the section of the numerical examples of the prior design are applied to calculation. Under such conditions, it is enough from the engineering viewpoint to examine up to as the number of struts.

The series of the values with one asterisk in Table 4.8 is one example of the optimal solution, which means the followings. The excavation progresses after building the first strut s_0 near the ground surface and if the first sign of failure appears when the depth of excavation reaches $3\,m$, the strut s_1 should be quickly constructed at $2.5\,m$ in depth. The cutting work is begun again after construction

Table 4. 8. Results of dynamic design procedure.

a_1 (m)	s_1* (m)	a_2 (m)	s_2* (m)	a_3 (m)	s_3* (m)	a_4 (m)	s_4* (m)	a_5 (m)	s_5* (m)
6	5.5	8	7.5	9	8.5				
		7	6.0	9	8.5				
				8	7.0	9	8.5		
5	4.5	8	7.5	9	8.5				
		7	6.5	9	8.5				
				8	7.0	9	8.5		
		6	5.0	9	8.5				
				8	7.0	9	8.5		
				7	6.0	9	8.5		
						8	7.0	9	8.5
4	3.5	8	7.5	9	8.5				
		7	6.5	9	8.5				
				8	7.0	9	8.5		
		6	5.0	9	8.5				
				8	7.5	9	8.5		
				7	6.0	9	8.5		
						8	7.0	9	8.5
		5	4.0	9	8.5				
				8	7.0	9	8.5		
				7	6.0	9	8.5		
						8	7.0	9	8.5
				6	5.0	9	8.5		
						8	7.0	9	8.5
						7	6.0	9	8.5
								8	7.5
3*	2.5	8	7.5	9	8.5				
		7	6.5	9	8.5				
				8	7.0	9	8.5		
		6*	5.5	9*	8.5				
				8**	7.0	9**	8.5		
				7	6.0	9	8.5		
						8	7.0	9	8.5
		5	4.5	9	8.5				
				8	7.0	9	8.5		
				7	6.0	9	8.5		
						9	7.0	9	8.5
				6	5.0	9	8.5		
						8	7.0	9	8.5
						7	6.0	9	8.5
								8	7.5
		4	3.0	9	8.5				
				8	7.0	9	8.5		
				7	6.0	9	8.5		
						8	7.0	9	8.5
				6	5.0	9	8.5		
						8	7.0	9	8.5
						7	6.0	9	8.5
								8	7.5
				5	4.0	9	8.5		
						8	7.0	9	8.5
						7	6.0	9	8.5
								8	7.5
						6	5.0	9	8.5
								8	7.5
								7	6.5

(Δa=1 m, a_{ult}=10m, steel sheet pile; SP-Ⅳ type)

of s_1 and if the failure is predicted again at $6\,m$ in depth, the strust s_2 is built at the location of $5.5\,m$. The further excavation is continued and if the engineer foresees the danger next time at $9\,m$ in depth, it becomes the best action for him to build the strut s_3 in short order at $8.5\,m$ in depth.

Let us next see the solutions with two asterisks in Table 4. 8. This is the case in which the third time indication of failure appears at $8\,m$ and the strut s_3 is built at $7\,m$ in depth in the above example. At that time, two possibilities exist. One is the possibility to be safely cut up to $10\,m$ with no more strut. In this case, the total number of struts is four including s_0. The other possibility is the case in which the sign of failure once more appears at $9\,m$ excavation and therefore one more s_4 at $8.5m$ in depth is needed. That is, five struts in all are built in this case. The Bayes' risk of both possibilities were calculated and compered, and as a result the latter solution was tabulated as the optimal solution because the Bayes' risk was smaller than the fomer one. But the following important fact should be noted. In the above example, the optimal location of s_3 when it becomes the final strut coincides with that of s_3 when one more s_4 is needed although the total Bayes' risk itself is a little different. This means that it is naturally not necessary for the engineers to built s_4 if there is actually no sign of failure in excavation after building s_3 at $7\,m$ in depth.

It is noteworthy in Table 4. 8 that the optimal location of the strut in each case becomes $(0.5\sim1.0)\,m$ higher than the bottom of excavation when the failure is predicted. These results can be said very common in the light of the past general excavation works which were based on the ripe experiences in engineering practice.

5. Conclusions

The main remarks of the present paper are summarized as follows;

(1) The undrained shear strength of saturated clay is classified into three typical types from the viewpoint of variation characteristics. It is shown that the undrained shear strength of each type can be regarded as a random variable which follows the normal distribution.

(2) The autocorrelation of the undrained shear strength of saturated clays is investigated. It is shown, based on practical data, that the autocorrelation coefficient in the vertical direction can be expressed by the exponential function of the distance of the positions.

(3) An embankment on poor ground is often constructed by the multistaged construction method. In doing so, it becomes very important in design to determine the transition process of the undrained strength of the clay layer. It is shown that the mean and coefficient of variation of the strength after consolidation can be derived from those of the initial state.

(4) There are two kinds of uncertainty in the stability analysis of slope. One is caused by the heterogeneity of natural ground and the other comes from the "analytical error" included in the conventional design method. Observations during construction provides information to improve both kinds of those uncertain conditions, whereas soil exploration data provide the information only on the state of natural ground.

(5) The information which show the mean shear stress on a potencial slip circle just before an actual failure is defined from observations during construction. The probability density function of a state of nature (a parameter vector of the distributions of ε and e, see Eqs. (3.1) and (3.2)) is improved by using the information during construction. These improvements are also formulated when there exists an observation error.

(6) When the vertical settlement d at the central place just under an embankment and the horizontal displacement δ near the toe of the slope are plotted on the $(d\sim\delta/d)$ diagram, it is shown that many practical embankments under different conditions failed near the one curve on this diagram and this curve is approached as construction progresses in failure cases whereas there is a tendency to be distant from this curve in non-failure cases.

(7) Many numerical analyses under the idealized conditions are carried out by using the finite element method after the accuracy of the calculation method is examined by comparing the calculated results with the observed results.

(8) The final failure points of the numerical examples on the $(d\sim\delta/d)$ diagram are investigated with those of observation, and it is shown that the failure criterion line in Fig. 3. 3 can represent well both the calculated and the observed results as a whole.

(9) The diagram for practical use of construction control is proposed in which several contour lines are added in order to know the degree of safety of the present situation under construction.

(10) Optimization of "Dynamic Design Procedure" of embankment construction is obtained from some numerical examples by minimizing the Bayesian predictive failure probability which is calculated by the improved probability density function of a state of nature.

(11) The methodology to deside the optimal type of earth retaining structure and the optimal arrangement of struct in the prior-design of excavation works is shown and some numerical examples are given. As the results of the numerical examples, it is found out that the optimal solutions in the prior-design give the very similar result to the actual past cases which were successfully completed by many engineer's ripe experience.

(12) The safety of earth retaining structure is investigated by many actual data observed in the field. As a result, $(y_{max}EI/pl^4)=\beta$ was adopted as the useful index to judge the degree of safety, where y_{max} denotes the maximum lateral deformation of the earth retaining structure which generally occurs near the bottom of the cut at the distance l from ground surface, p the intensity of the lateral earth pressure at the same point and EI the bending rigidity of the earth retaining structure.

(13) The rate of change of $\log\beta$ with progress of excavation is quantitatively investigated and it is clarified that $\log\beta$ generally decreased monotonously against the cutting depth D. In addition, the relation of $\log\beta$ and D is discussed from the actual situation in the construction field and it is concluded reasonable that this relation shows the contour of the degree of safety during construction.

(14) On the basis of above stated results, the diagrams for construction control are separately proposed for the different types of earth retaining structure.

(15) The "Dynamic Design Procedure" in which the results of the prior design are modified by new information obtained during construction is applied to the excavation problem. The "Dynamic Design Procedure" which is firstly formulated

for the embankment problem is modified so as to be applied to the excavation problem and the results obtained from the numerical studies are also compared with those actually obtained hitherto through the course of excavation works.

References

1) Benjamin, J. R. and Cornell, C. A. (1970): "Probabilities, Statistics and Decison for Civil Engineers," McGraw-Hill, pp. 524-594.
2) Bishop, A. W. and Bjerrum, L. (1960): "The relevance of the triaxial test to the solution of stability problems," Proc. of Research Conf. on Shear Strength of Cohesive Soil, ASCE., pp. 437-501.
3) Bjerrum, L. and Eide, O. (1956): "Strutted Excavation in Clay," Geotechnique, Vol. 6.
4) Burland, J. B. (1971): "A method of estimating pore pressures and displacements beneath embankments on soft natural deposits," Proc. Roscoe Mem. Sym., pp. 505-536.
5) D'Appolonia, D. J. and Lambe, T. W. (1970): "Method for predicting initial settlement," ASCE, Vol. 96, No. SM 2, pp. 523-544.
6) Davis, E. H. and H. G. Poulos, (1968): "The use of elastic theory for settlement prediction under three-dimensional conditions." Geotechnique, Vol. 18, No. 1, pp. 67-91.
7) Diaz Pedilla, J. and Vanmarcke, E. H. (1974): "Settlement of structures on shallow foundations, a probabilistic approach," M.I.T. Dept. of Civil Eng., Research Report, R 74-9.
8) Duncan, J. M. and Chang, C. Y. (1970): "Nonlinear analysis stress and strain in soil," ASCE, Vol. 96, No. SM 5, pp. 1629-1653.
9) Foloyan, J. I., Hoeg, K. and Benjamin, J. R. (1970): "Decision theory applied to settlement predictions," J. Soil Mech, and Found. Div., ASCE., 96, SM 4, pp. 1127-1141.
10) Höeg, K., Christian, J. T. and Whitman, R. V. (1968): "Settlement of strip load on elastic-plastic soil," ASCE, Vol. 94, No. SM 2, pp. 43-445.
11) Hooper, J. A. and Butler, F. G. (1966): "Some numerical results concerning the shear strength of London Clay," Geotechnique, Vol. 16, pp. 282-304.
12) Kotoda, K. and Mori, S. (1974): "Comparison of Rankine earth pressure with measured earth pressure on earth retaining structure," Proc. of Annual Conf. on JSSMFE, pp. 797-800 (in Japanese).
13) Kurihara, N. (1972): "The Probabilistic approach to design of embankment," Technical Report of Japanese Highway Public Corporation, pp. 75-85.
14) Lumb, P. (1966): "The Variability of natural soils," Canadian Geotechnical Journal, Vol. 3, pp. 74-97.
15) Lumb, P. (1970): "Safety factors and the probability distribution of strength," Canadian Geotechnical Journal, Vol. 7, pp. 225-242.
16) Lumb, P. and Holt, J. K. (1970): "The undrained shear strength of a soft marine clay from Hong Kong," Geotechnique, Vol. 18, pp. 25-36.
17) Matsuo, M. and Asaoka, A. (1974): "A statistical approach to settlement prediction," Proc. JSCE, No. 225, pp. 63-74.
18) Matsuo, M. and Asaoka, A. (1975): "A study on the optimum design for multistaged construction of embankment," Proc. JSCE, No. 240, pp. 35-49.
19) Matsuo, M. (1976): "Reliability in embankment design," M.I.T. Dept. of Civil Eng., Research Report pp. 1-203.
20) Matsuo, M. and Asaoka, A. (1976): "A statistical study on a conventional safety factor method," Soils and Foundations, Vol. 16, No. 1, pp. 75-90.
21) Matsuo, M. and Asaoka, A. (1977): "Probability models of undrained strength of marine clay layer," Soils and Foundations, Vol. 17, No. 3, pp. 1-16.
22) Matsuo, M. and Asaoka, A. (1978): "Dyamic design philosophy of soils based on the

Bayesian reliability prediction," Soils and Foundations, Vol. 18, No. 4, pp. 1-11.
23) Matsuo, M. and Kawamura, K. (1975): "Study on modified method of design of embankment by observation during construction," Proc. JSCE, No. 240, pp. 113-123.
24) Matsuo, M. and Kawamura, K. (1977): "Diagram for construction control of embankment on soft ground," Soils and Foundation, Vol. 17, No. 3, pp. 37-52.
25) Matsuo, M. and Kawamura, K. (1980): "A design method of deep excavation in cohesive soil based on the reliability theory," Soils and Foundations, Vol. 20, No. 1, pp. 61-75.
26) Matsuo, M. and Kawamura, K. (1980): "Prediction of failure of earth retaining structure during excavation work," Soils and Foundations, Vol. 20, No. 3.
27) Matsuo, M. and Kuroda, K. (1971): "Study on the soil exploration system for stability analysis of embankment," Proc. JSCE, Vol. 198, pp. 75-86.
28) Matsuo, M. and Kuroda, K. (1972): "A stochastic study on some properties and failure probability for unsaturated soils," Proc. JSCE, Vol. 208, pp. 65-75.
29) Matsuo, M. and Kuroda, K. (1974): "Probabilistic approach to design of embankments," Soils and Foundations, Vol. 14, No. 2, pp. 1-17.
30) Matsuo, M. and Kuroda, K. (1975): "Economical evaluation of embankment design," Soils and Foundations, Vol. 15, No. 2, pp. 31-46.
31) Matsuo, M., Kuroda, K. and Asaoka, A. (1975): "Uucertainties and decision in design of embankment," Proc. of 2nd International Conference on Application of Statistics and Probability in Soil and Structural Engineering, pp. 143-153.
32) Matsuo, M., Kuroda, K., Asaoka, A. and Kawamura, K. (1977): "Dynamic decision procedure of slope construction," Proc, of 9th ICSMFE, Vol. 2, pp. 177-120.
33) Meyerhof, G. G. (1970): "Safety factors in soil mechanics," Canadian Geotechnical Journal, Vol. 7, No. 4, pp. 349-355.
34) Muromachi, T. and Watanabe, S. (1962): "Deformation of soft peat foundation under embankment," Railway Technical Research Report, No. 154, pp. 1-49 (in Japanese).
35) Peck, P. B. (1969): "Deep Excavations and Tunnelling," 7th Intern. Conf. SMFE, the State of Art, pp. 259-290.
36) Raiffa, H. and Schlaifer, R. (1961): "Applied statistical decision theory," Division of Research, Graduate School of Business Administration, Harvard Univ.
37) Schultze, E. (1971): Frequency distributions and correlation of soil properties, statistics and probability in civil engineering," (Ed. P. Lumb), Hong Kong, Hong Kong University Press.
38) Schultze, E. (1975): "Some aspects concerning the application of statistics and probability to foundation structures," Proc. 2nd International Conference on Application of Statistics and Probability in Soil and Structural Engineering, pp. 457-494.
39) Terzaghi, K. and Pcck, R. B. (1967): "Soil mechanics in engineering practice," New York, John Wilcy and Sons.
40) Tschebotarioff, G. P. (1951): Soil mechanics, foundation, and earth structure," McGraw-Hill, p. 655.
41) Vanmarcke, E. H. (1977): "Probabilistic modelling of soil profile," Proc. of the Specialty Session, No. 6 of 9th ICSMIFE.
42) Wu, T. H. and Kraft, L. M. (1967): "The probability of foundation safety," Proc. ASCE, Vol. 93, SM5, pp. 213-231.
43) Wu, T. H. (1974): "Uncertainty, safety and decision in soil engineering," Proc., ASCE, GT 3, pp. 329-348.
44) Yamagata, K., Yoshida, Y. and Akino ,N. (1969): "On the lateral supports in temporary open cuts," Tsuchi-to-Kiso, JSSMFE, Vol. 17, 9, pp. 33-45 (in Japanese).
45) Yamaguchi, H. and Murakami, Y. (1976): "Plane strain consolidation of a clay layer with finite thickness," Soils and Foundations, Vol. 16, No. 3, pp. 66-79.